ISSN 1063-7729, Astronomy Reports, 2015, Vol. 59, No. 7, pp. 591–625. © Pleiades Publishing, Ltd., 2015.

Black Holes, Supernovae and Gamma Ray Bursts*

Remo Ruffini**

Dip. di Fisica, Sapienza Univ. and ICRA, P.le A. Moro 5, I-00185 Rome, Italy
ICRANet, Piazzale della Repubblica 10, I-65122 Pescara, Italy
Univ. de Nice Sophie Antipolis, Nice, Grand Château Parc Valrose, France
ICRANet Rio—CBPF, Rua Doutor Xavier Sigaud 150, Rio de Janeiro, Brazil

Received January 26, 2015

Abstract—A tribute to Ya.B. Zel'dovich in the occasion of the 100th anniversary of his birth. The three fundamental paradigms for the gamma-ray burst and supernova connections to neutron stars and black holes are outlined.

DOI: 10.1134/S1063772915070082

1. INTRODUCTION AND THE FIRST PARADIGM

Supernovae (SNe) have been known and studied for a long time, from 1054, to the classic works of Baade and Zwicky in 1934 [1, 2] and of Oppenheimer and his students in 1939, to the detection of a pulsar, first in the radio and then in the optical wavelength, at the center of the Crab Nebula, in 1968. The explanation of the energetics of pulsars as originating from the rotational energy of neutron stars have given the first clear evidence for the existence of neutron stars and has lead to the conclusion that the Crab supernova originated from the gravitational collapse to a neutron star. The next fundamental discovery came from the pioneering work of Riccardo Giacconi and his group with the detection in X-Ray Astronomy of Sco X-1 [3]. In 1967 this results were theoretically interpreted by Shklovskii [4] as originating from a binary system with a neutron star as a member. These results were followed by the launch of the UHURU satellite on December 12, 1970. The coordination of the X-ray observations with the observations from optical telescopes from the ground has lead to the discovery a large number of Binary X-Ray sources in our galaxy [5]. These systems gave evidence for: (a) an emission in the X-ray due to accretion in a binary system composed of massive star and a gravitational collapsed star, such X-Ray luminosities, originating in gravitational energy, was million times more intense than ones expected from the stars thermonuclear evolution; (b) the first determination of neutron star masses well above the critical mass value expected by Oppenheimer and Volkoff, see, e.g., Cen X-3 on Fig. 1 and (c) the first identification of a black hole in Cygnus X-1 [6–8].

Observations of GRBs only date from the detection by the Vela satellites in the early 1970s, see e.g. [9] and references therein. It has only been after the observations in 1997 by the Beppo-SAX satellite [10], which have allowed the optical identification of GRBs, by the estimate of their cosmological distance, that their enormous energetics, 10^3-10^4 times larger than those of SNe, have been determined: energies of the order of 10^{54} erg, equivalent to the release of $\sim M_\odot c^2$ in few tens of seconds. This result was predicted on pure theoretical ground assuming that GRBs originated by the electron positron plasma originating in the gravitational collapse to a Kerr–Newman black hole already in 1975 [11]. Out of these experiences I had formulated a basic paradigm to serve as guideline to interpret unitarily and consistently the occurrence of Supernovae, the existence of binary X-Ray source and also possibly the nature of GRBs [12–14].

As we will see the enforcement of this minimal set of assumptions has been extremely valuable. As the knowledge of these systems has evolved I introduced two new and more specific paradigms narrowing in on the nature of the sources: each new paradigm being clearly in agreement with the previous ones. I was well aware of a vast literature contemplating the possibility of relating different Supernovae types to black holes in a very vast range of masses: I was very doubtful on these considerations since they were

*The text was submitted by the author in English.

**E-mail: ruffini@icra.it

Paper was presented at the international conference in honor of Ya.B. Zeldovich 100th Anniversary "Subatomic Particles, Nucleons, Atoms, Universe: Processes and Structure" held in Minsk, Belarus, in March 10–14, 2014. Published by the recommendation of the special Editors: S.Ya. Kilin, R. Ruffini, and G.V. Vereshchagin.

violating more then one principle of my paradigm, they neglected a wealth of observational data and were based on a somewhat restrictive property related to metallicity in the thermonuclear evolution expected in a single star system (see e.g. [15]). Moreover, today we start to understand, after the splendid observations of the Space Telescope [16], that even Eta Carinae is a binary system [17, 18] and that massive single stars are very likely a set of measure zero: massiveness implies multiplicity.

First paradigm

- *Supernovae (SN) originate from the gravitational collapse to a neutron star.*
- *GRBs originate during the gravitational collapse to a black hole (BH).*
- *In considering a massive star its binary nature and possibly its multiple system should be duly and necessarily considered.*

This situation has become even more interesting after the unexpected observation of a temporal and spatial coincidence between the occurence of a GRB and a SN explosion, see e.g. GRB 980425 [19] and SN 1998bw [20, 21]. The explanation of this coincidence has led our group to introduce the Induced Gravitational Collapse (IGC) paradigm (paradigm 1), a many-cosmic-body-interaction, and consequently we introduced a Cosmic Matrix: a C-Matrix; see Fig. 2. The many-particle interaction in the S-Matrix is confronted with this new concept of C-Matrix involving a many-body interaction among astrophysical systems. This unprecedented situation has lead to a series of new conceptual paradigms and the opening of a new understanding of a vast number of unknown domains of physics and astrophysics, see e.g. [22] and references therein.

In all this a work pioneered by Zel'dovich has gained a particular new interest [24]. What is most extraordinary is that I discovered this article by accident while I was departing for Minsk for the celebration of his 100th anniversary. This is one of the usual dialogue with him which still occur , in a mysterious way. I will dedicate this talk to him and recall some other anecdotes in addition to the ones I already mentioned in the occasion of the the celebration of his 95th anniversary [25].

1.1. CRAB Pulsar: NS and BH

That NSs exist in nature has been proven by the discovery of Pulsars. The year 1967 marked the discovery of the first pulsar, observed at radio wavelengths in November 28, 1967 by Jocelyn Bell Burnell and Antony Hewish [26]. Just a few months later, the Pulsar NP0532 was found in the center of the Crab Nebula and observed first at radio wavelengths and soon after at optical wavelengths. The discovery of NSs led our small group working around John Wheeler in Princeton to direct our main attention to go further and adress the study of continuous gravitational collapse to a BH introduced by Oppenheimer and his students (see Fig. 4). The work in Princeton addressed the topic of BHs, Gravitational Waves (GWs) and cosmology. A summary of that work can be found in [27, 28], where a vast number of topics of Relativistic Astrophysics was reconsidered, including the possible sources of GWs, the cross-sections of GW detectors, and especially, an entirely new family of new astrophysical phenomena occurring around NSs and BHs and in cosmology.

One of the most important results in the physics and astrophysics of BHs has been the BH mass-energy formula (see Fig. 5). From this, indeed, it became clear that up to 50% of the mass-energy of a BH could be extracted by using reversible transformations [30]. It then followed that during the formation of a BH, some of the most energetic processes in the Universe should exist, releasing an energy of the order of $\sim 10^{54}$ erg for a 1 $M_\odot$ BH (see Fig. 5).

1.2. The VELA and CGRO Satellites and GRBs

In [31] I described how the observations of the Vela satellites were fundamental in discovering GRBs, see Fig. 6. Just a few months after the public announcement of their discovery [9], with T. Damour, a collaborator in Princeton, I formulated a theoretical model based on the extractable energy of a Kerr–Newmann BH through a vacuum polarization process as the origin of GRBs, see Fig. 7. In our paper [11], we pointed out that vacuum polarization occurring in the field of electromagnetic BHs could release a vast e^+e^-

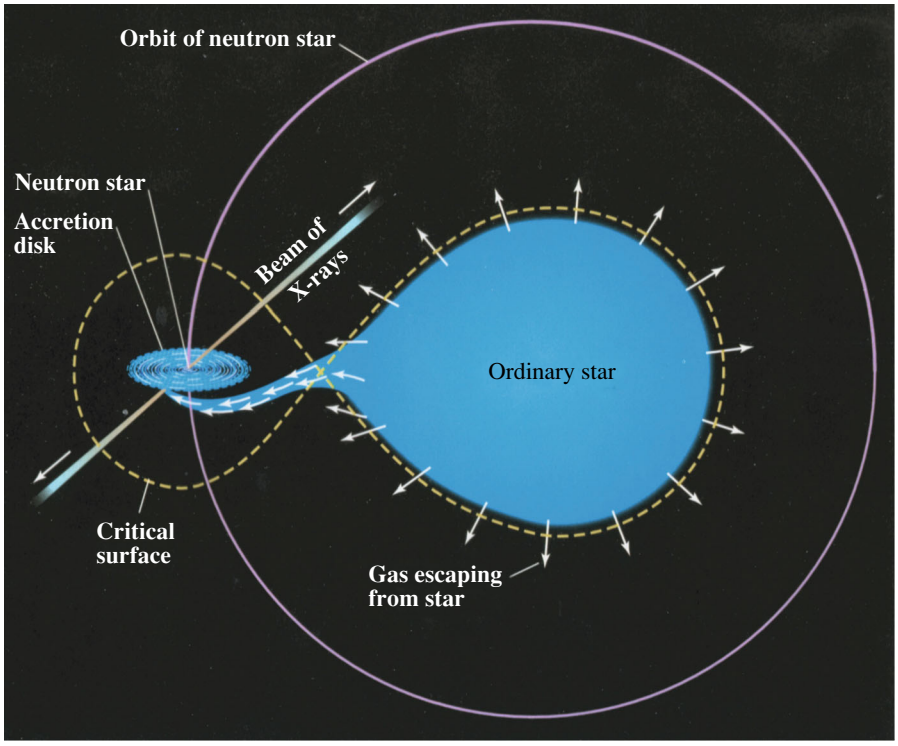

Fig. 1. X-ray binary Centaurus X3 detected by UHURU satellite. The pulse period is 4.84 s. Binary motion signature has been found with orbital period 1.7 days, with credit to UHURU.

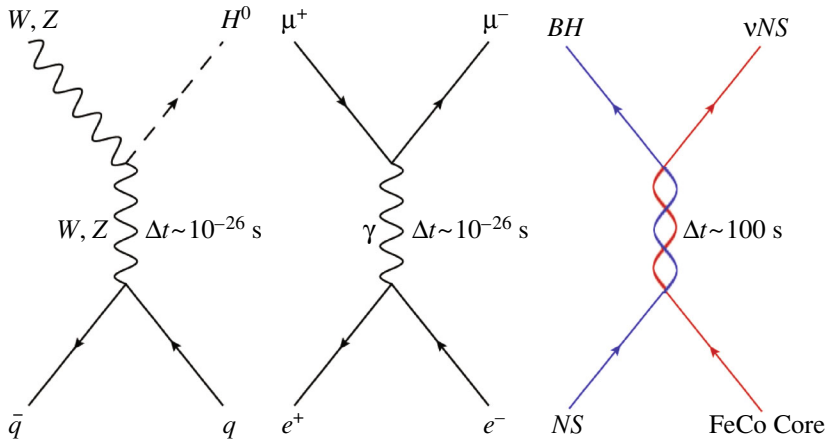

Fig. 2. The new concept of "C-Matrix," compared with the usual S-Matrix. From [23].

plasma which self-accelerates and gives origin to the GRB phenomenon. Energetics for GRBs all the way up to $\sim 10^{55}$ erg was theoretically predicted for a 10 $M_\odot$ BH [12]. The dynamics of this e^-e^+ plasma was first studied by J.R. Wilson and myself with the collaboration of S.-S. Xue and J.D. Salmonson [32, 33].

Initially it was difficulty to model GRBs to understand their nature since their distance from the Earth was unknown, and thousands of models were presented [34] attempting to explain the mystery they presented. The launching of the CGRO Satellite with the BATSE detectors on-board (see Fig. 8) led to the following important discoveries:

(1) the homogeneous distribution of GRBs in the Universe;

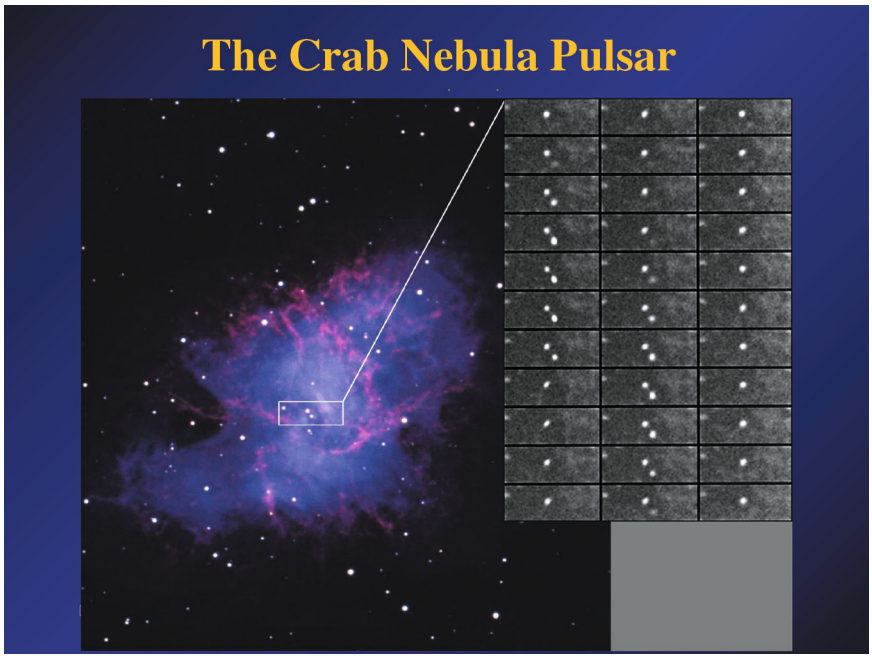

Fig. 3. The sequence of black and white images on the right is separated by one millisecond intervals, from which it is clear that the left star is a pulsar with a period of $P = 33$ milliseconds. This period changes with a rate dP/dt of 12.5 microseconds per year. The fact that the loss of rotational energy of a neutron star with moment of inertia I is given by $dE/dt \propto -I(1/P^3)dP/dt$ explains precisely the energetics of the pulsar and proves at once the existence of NSs [29].

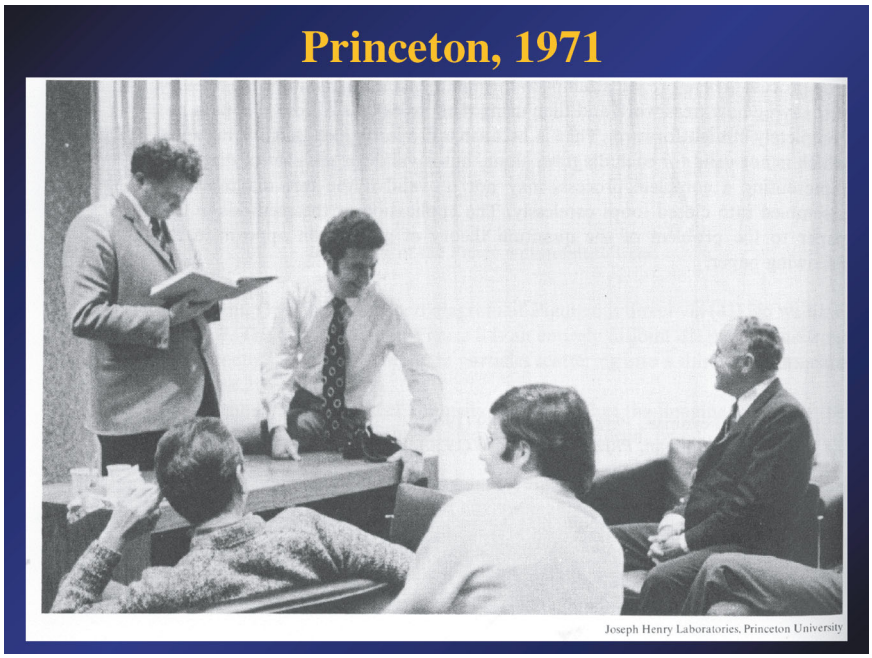

Fig. 4. Standing to the left Tullio Regge, sitting on the desk myself and sitting on the chair John Wheeler.

(2) the existence of short GRBs lasting less than a second ; and

(3) the existence of long GRBs, lasting more than one second.

The crucial contribution to interpreting GRBs came from the Italian–Dutch Beppo-SAX satellite, see Fig. 9 (e.g. [36]) which led to a much more precise definition of their position in the sky obtained using a wide field X-ray camera and narrow field instrumentation. This enabled the optical identification of GRBs

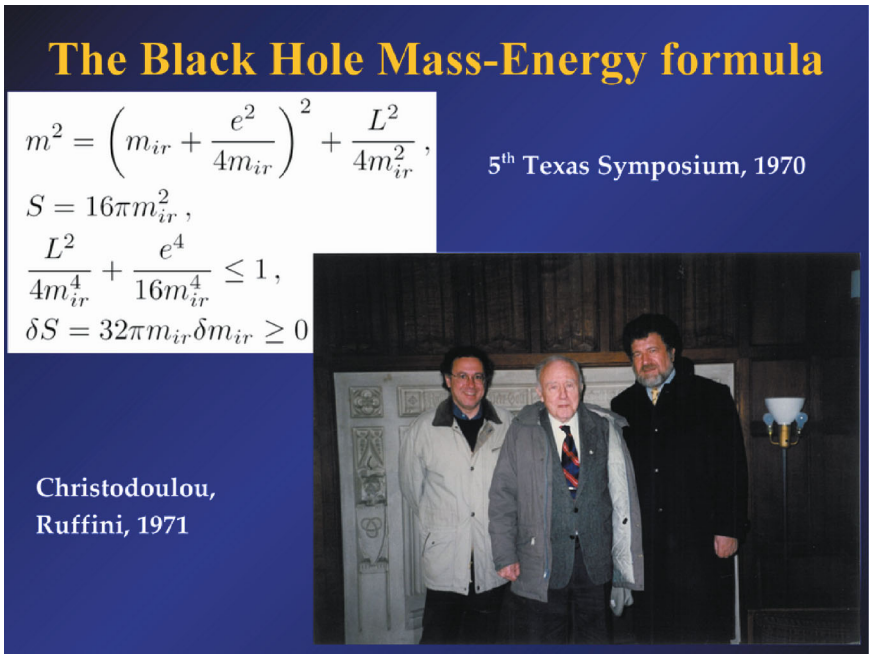

Fig. 5. The black hole mass-energy formula. From [30].

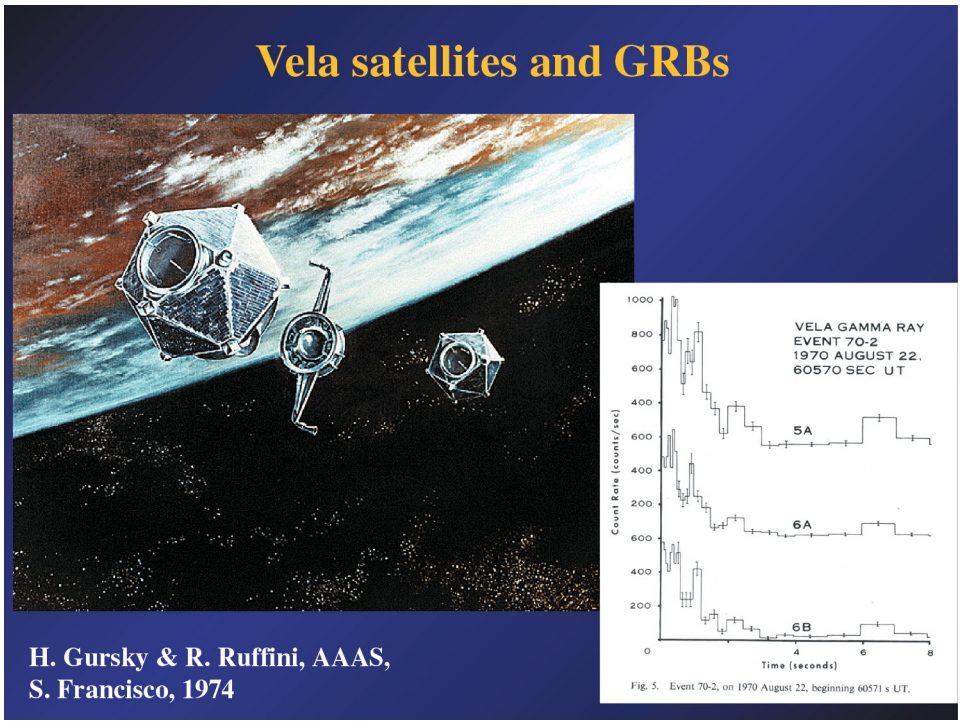

Fig. 6. The Vela satellites, see e.g. the Ian Strong chapter in [9].

and the determination of their cosmological redshift, and consequently of their energetics, which turned out to be up to $\sim 10^{55}$ erg, precisely the one predicted by Damour and myself in [11]. Since that time no fewer than ten different X- and γ-ray observatory missions and numerous observations at optical and radio wavelengths have allowed us to reach a deeper understanding of the nature of GRBs, see Fig. 9.

1.3. Some Work of Zel'dovich and the Soviet School on an Hypercritical Accretion

I have already remembered in my article [25] some of the anecdotes of my encounters with Zel'dovich

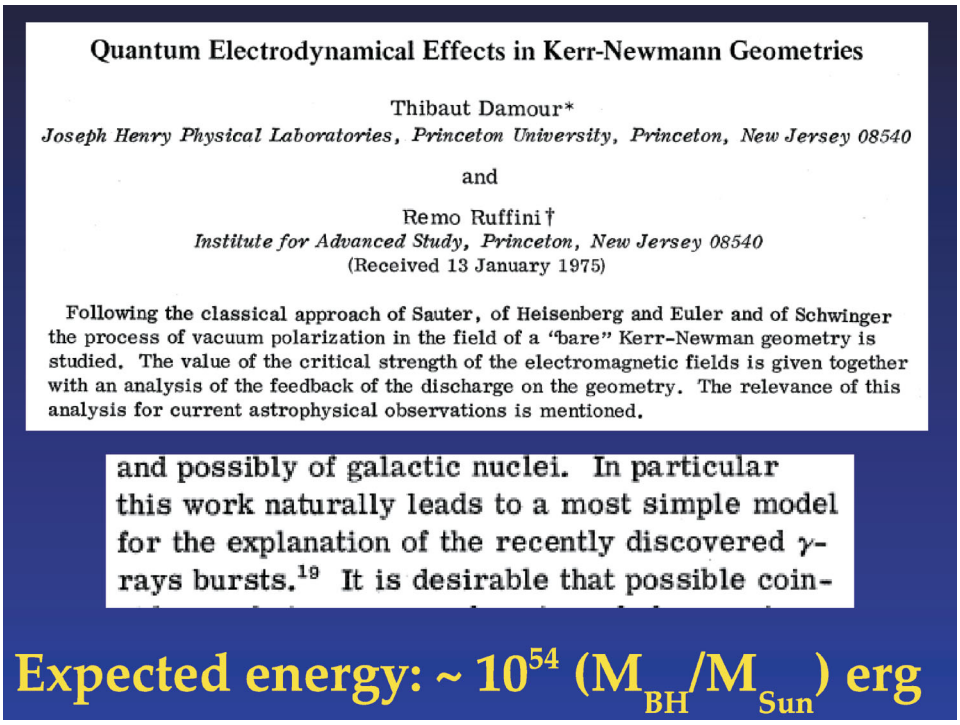

Fig. 7. The classic paper [11] on the extractable energy of a Kerr–Newmann BH through vacuum polarization.

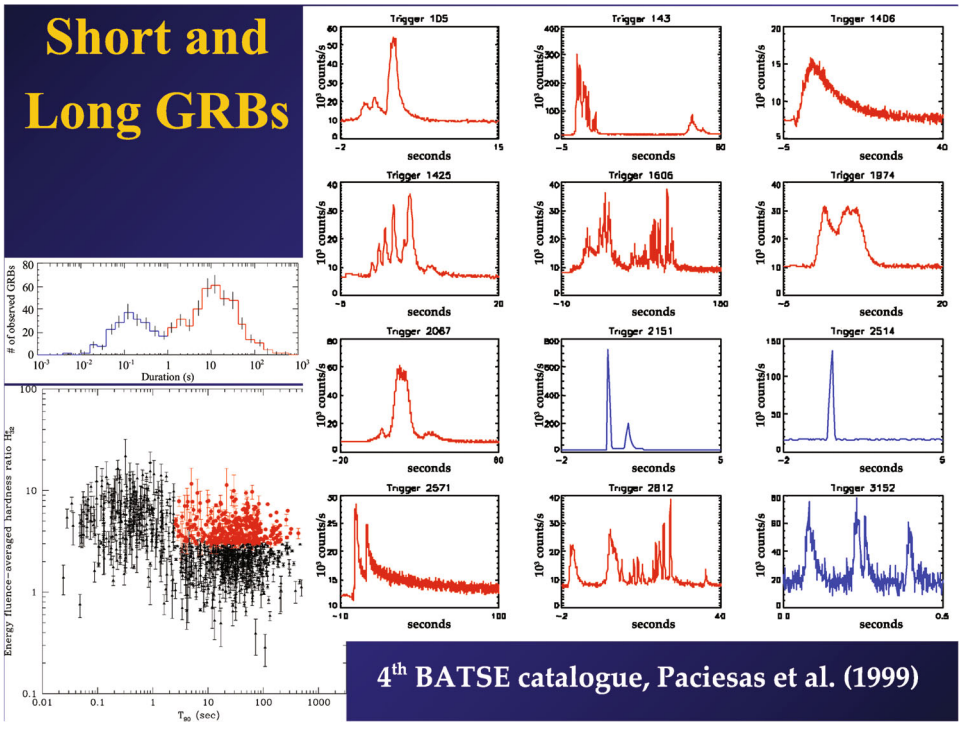

Fig. 8. Short and long GRB light curves and their temporal distribution from the 4th BATSE catalog, [35].

including the pictures of our memorial encounter with the Pope John Paul II and the many meetings with Sakharov and Bruno Pontecorvo a thruly giant figure in the study of neutrino physics and astrophyiscs. I had only here the last picture I took myself of Zel'dovich and Pontecorvo, see Fig. 10. Recently

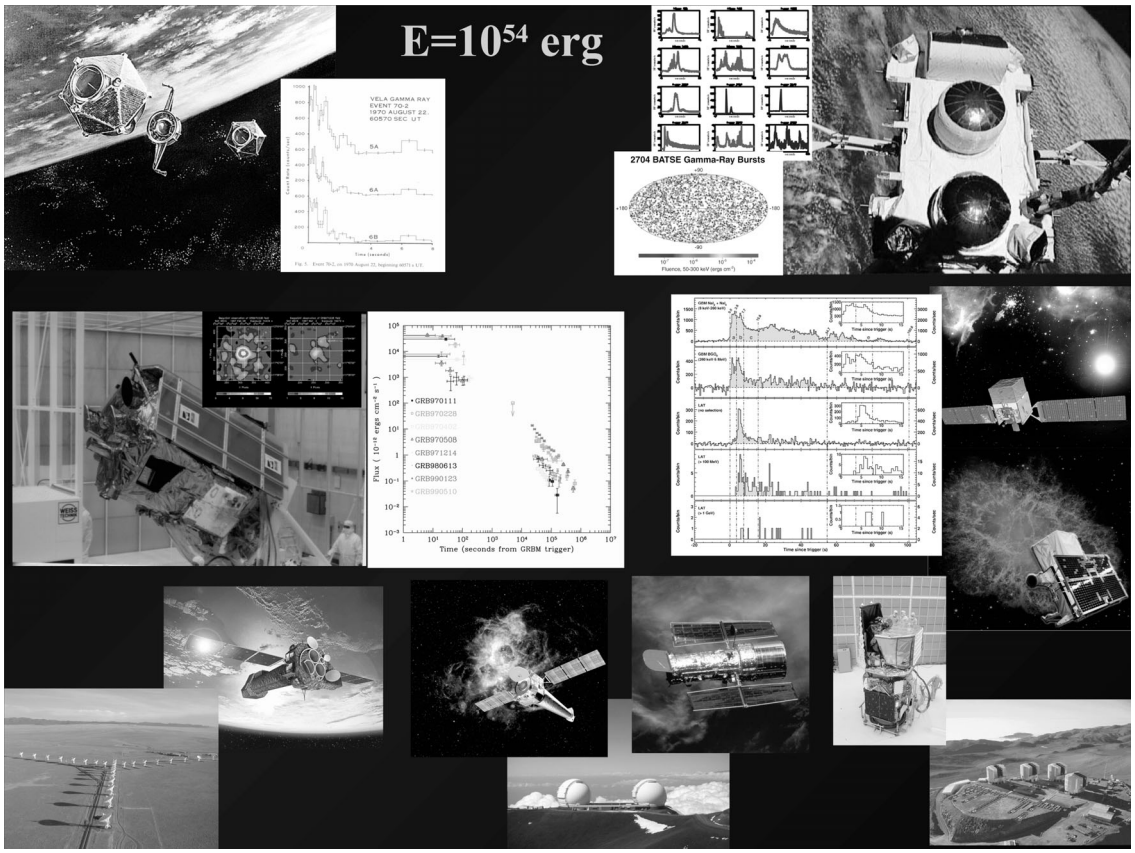

Fig. 9. The flottila of space missions and the main astronomical optical and radio observatories who have participated in establishing the cosmological distance and energetics of GRBs extending up to the limit of 10^{55} erg predicted in 1975, see Fig. 7. Most significant has been the central role of the mission Beppo Sax by the coordinate observations of the narrow high energy field instruments and the Wide Field X-ray cameras, which were financed on the limited funds of the scientific committee of ASI. This mission has allowed the discovery of the prolonged GRB emission and consequently the optical identification of the GRBs sources.

by chance I came across a paper by Zel'dovich, Ivanova and Nadezhin in which the non stationary hydrodinamical accretion onto a Neutron Star was considered [24]. There the case of an optically thick gaseous cloud of $10^{-5}\ M_\odot$ accretion onto a Neutron Star was considered taking into account the radiative thermal conduction and neutrino emission. The characteristic contraction time is there determined by the energy losses due to neutrinos emission. The case of accretion of a massive cloud of the order of $1\ M_\odot$ are there considered and shown that almost all gravitational energy of the cloud is emitted in the form of neutrinos.

This work months later was paralleled by one I did with Jim Wilson [37]. There we were motivated by the analysis of binary X-ray sources such as Cen X-3 or Cygnus X-1 we were studying at the time, see e.g. Giacconi and Ruffini [38] and references therein, where the X-ray luminosities are observed to be in the range $10^{37}-10^{38}$ erg/s with typical matter accretion less then $5\times10^{-7}M_\odot$/year. With Jim we looked at the problem of super-Eddington accretion and concluded that neutrino emission could allow accretion rates in neutron stars much larger then the critical value obtained from a straightforward application of the Eddington limit and in these cases the neutrino luminosity originating from pair annihilation will be much larger then the electromagnetic energy in X-ray although not be detectable for typical galactic sources. We abandoned this research although the conceptual basis for estimating neutrinos emission in hyper-accreting neutron stars was there clearly identified. I had occasion to present these results to Zel'dovich in Moscow, as we acknowledged in our manuscript, and he agreed with the correctness of our estimate on the ground of his previous work which I now understand was the work with Ivanova and Nadezhin.

It is very curious that both these works did not encounter astrophysical interest at the time and were left as elegant theoretical exploration without a direct application. I am going to show later in this presenta-

Fig. 10. Picture taken by myself in an unplanned visit to an hospital in Moscow. On the left side Zeldovich, on the right side Pontecorvo.

tion that indeed these works have become crucial and are at the basis of our most recent developments in the understanding of the GRBs as well as supernovae in the case of the association of Supernovae and GRBs.

After reviewing in the next paragraphs the basic differences between the most quoted "fireball model" of GRBs and our "fireshell model," I will describe induced Gravitaional collapse paradigm (the "second paradigm") and the analysis of the GRB 090618 in the fireshell scenario [39]. This will show the first application of the IGC paradigm to it [40]. I will then indicate some recent results on a possible distance indicator inferred from a GRB-SN correlation within the IGC paradigm [41], then giving some additional evidence coming from the identification of the neutron star created by the SN and its use as a cosmological candle. I will turn to the first examples of genuine short GRB 090227B [42] leading to a BH formation. Finally I will illustrate a brand new paradigm dealing with the two families of short and long GRBs and a special role of the formation or absence of a black hole.

1.4. The Fireball Model Compared and Contrasted to the Fireshell Model

A variety of models have been developed to theoretically explain the observational properties of GRBs, among which the Fireball model [43] is one of those most often used. In [44–47] it was proposed that the sudden release of a large quantity of energy in a compact region can lead to an optically thick photon-lepton plasma and to the production of e^+e^- pairs. The sudden initial total annihilation of the e^+e^- plasma was assumed by Cavallo and Rees [44], leading to an enormous release of energy pushing on the CBM: the "fireball" (see Fig. 11).

An alternative approach, originating in the gravitational collapse to a BH, is the Fireshell model, see e.g. [48, 49]. Here the GRB originates from an optically thick e^+e^- plasma in thermal equilibrium, with a total energy of $E_{\rm tot}^{e^\pm}$. This plasma is initially confined between the radius r_h of a BH and the dyadosphere [50, 51] radius

$$r_{ds} = r_h \left[2\alpha \frac{E_{\rm tot}^{e^+e^-}}{m_e c^2} \left(\frac{\hbar/m_e c}{r_h} \right)^3 \right]^{1/4}, \qquad (1)$$

where α is the usual fine structure constant, $\hbar$ the Planck constant, c the speed of light, and m_e the mass of the electron. The lower limit of $E_{\rm tot}^{e^\pm}$ is assumed to coincide with the observed isotropic energy $E_{\rm iso}$ emitted in X-rays and gamma rays alone in the GRB. The condition of thermal equilibrium assumed in this model [52] distinguishes this approach from alternative ones, e.g. [44].

1.4.1. The Fireball model. In the Fireball model, the prompt emission, including the sharp luminosity variations [53], are caused by the prolonged and variable activity of the "inner engine" [43, 54]. The conversion of the fireball energy to radiation originates in shocks, either internal (when faster moving matter overtakes a slower moving shell, see [54]) or external (when the moving matter is slowed down by the external medium surrounding the burst, see [55]).

Much attention has been given to synchrotron emission from relativistic electrons in the CBM,

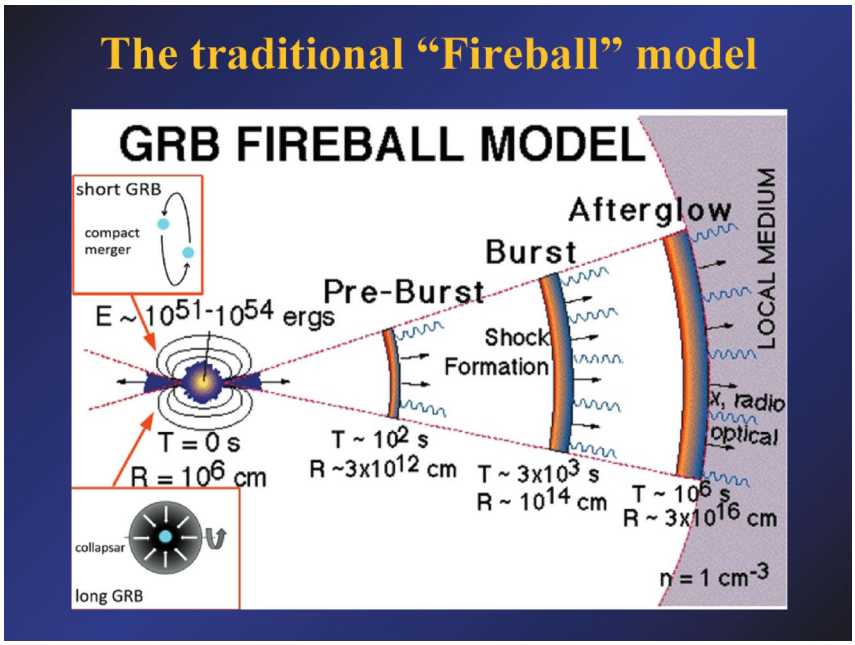

Fig. 11. The traditional "Fireball" model. See e.g. [47] and references therein.

possibly accompanied by Self-Synchrotron Compton (SSC) emission, to explain the observed GRB spectra. These processes were purported to be consistent with the observational data of some GRBs [56, 57]. However, several limitations have been reported in relation with the low-energy spectral slopes of time-integrated spectra [58–61] and the time-resolved spectra [61]. Additional limitations on SSC emission have also been pointed out in [62, 63].

The latest phases of the afterglow are described in the Fireball model by a single ultrarelativistic jetted emission assuming an equation of motion given by the Blandford–McKee self-similar power-law solution [64]. The maximum Lorentz factor of the fireball is estimated from the temporal occurrence of the peak of the optical emission, which is identified with the peak of the forward external shock emission [65, 66] in the thin shell approximation [67].

Several partly alternative and/or complementary scenarios have been developed distinct from the Fireball model, e.g. based on quasi-thermal Comptonization [68], Compton drag emission [69, 70], synchrotron emission from a decaying magnetic field [71], jitter radiation [72], Compton scattering of synchrotron self-absorbed photons [73, 74], and photospheric emission [75–81]. In particular, it was pointed out in [80] that photospheric emission overcomes some of the difficulties of purely non-thermal emission models. The collapsar model, leading to the astrophysical framework of the "fireball" model characterized by a jetted ultrarelativistic (Lorentz Gamma Factor 100–500) emission, was then introduced (see Fig. 11).

1.4.2. The Fireshell model. Let us turn to the fireshell model. There, the rate equation for the e^+e^- pair plasma and its dynamics (the pair-electromagnetic pulse or PEM pulse for short) have been described in [32, 33]. This equation applies to any electron-positron plasma originating the GRB phenomena, quite independently if generated by vacuum polarization around a Kerr–Newman BH [11] or other mechanisms e.g. electron positron pairs originated in neutrinos antineutrinos annichilation mechanism. This plasma engulfs the baryonic material left over from the process of gravitational collapse having a mass M_B, still maintaining thermal equilibrium between electrons, positrons, and baryons.

The baryon load is measured by the dimensionless parameter $B = M_B c^2/E_{\rm tot}^{e^+e^-}$. [33, 82] showed that no relativistic expansion of the plasma exists for $B > 10^{-2}$, see Fig. 12. The fireshell is still optically thick and self-accelerates to ultrarelativistic velocities (the pair-electromagnetic-baryonic pulse or PEMB pulse for short [33, 82]). Then the fireshell becomes transparent and the P-GRB is emitted [83]. The final Lorentz gamma factor at transparency can vary over a wide range between 10^2 and 10^4 as a function of $E_{\rm tot}^{e^+e^-}$ and B.

For its final determination it is necessary to explicitly integrate the rate equation for the e^+e^- annihilation process and evaluate, for a given BH mass

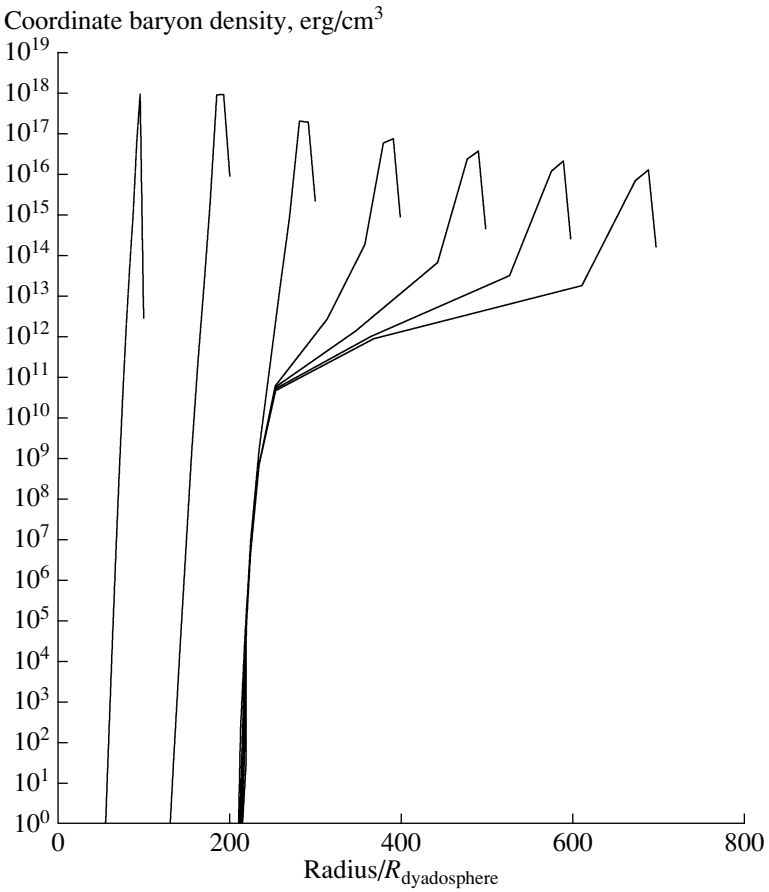

Fig. 12. The turbulent expansion for $B = 10^{-2}$. See details in [33].

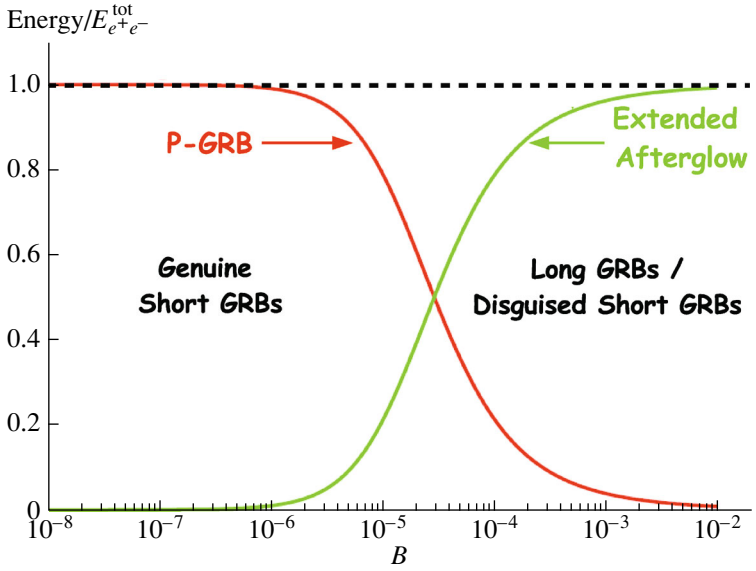

Fig. 13. The energy emitted in the extended afterglow (solid green curve) and in the P-GRB (solid red curve) in units of $E^{\rm tot}_{e^+e^-} = 1.77 \times 10^{53}$ erg (dashed horizontal line), as functions of B. The crossing point, corresponding to the condition $E_{(P-GRB)} \equiv 50\% E^{\rm tot}_{e^+e^-}$, marks the division between the genuine short and the disguised short and long GRB regions. The upper limit of 10^{-2} for B is determined by the onset of instabilities as shown in Fig. 12. From [42].

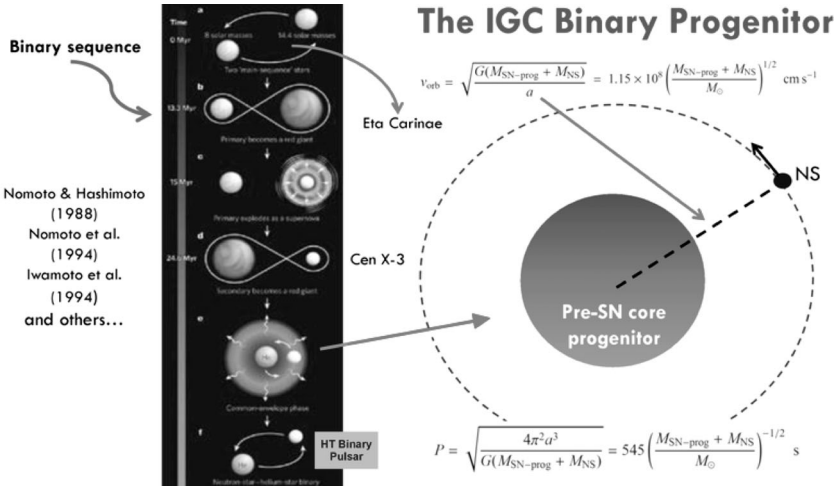

Fig. 14. The IGC binary progenitor. For details see [40, 99].

and a given e^+e^- plasma radius, at what point the transparency condition is reached [33].

The fireshell scenario does not require any prolonged activity of the inner engine and applies in generality to any confined amount of e^+e^- in a dyadosphere. After transparency, the remaining accelerated baryonic matter still expands ballistically and starts to slow down from collisions with the CBM of average density n_{CBM}. In the standard fireball scenario [47], the spiky light curve is assumed instead to be caused by internal shocks.

In the fireshell model the entire extended-prompt emission is assumed to originate from an expanding thin baryonic shell, which maintains energy and momentum conservation during its collision with the CBM. The condition of a fully radiative regime is assumed [83]. This in turn allows one to estimate the characteristic inhomogeneities of the CBM, as well as its average value. It is appropriate to point out another difference between our treatment and others in the current literature. The complete analytic solution of the equations of motion of the baryonic shell were developed in [84, 85], while elsewhere the Blandford–McKee self-similar approximate solution is almost always adopted without justification [77, 86–94]. The analogies and differences between the two approaches have been explicitly explained in [95].

In our general approach, a canonical GRB bolometric light curve is composed of two different parts: the P-GRB and the prompt radiation phase. The relative energetics of these two components and the observed temporal separation between the corresponding peaks is a function of the above three parameters $E_{\rm tot}^{e^+e^-}$, B, and the average value of the n_{CBM}. The first two parameters are inherent to the accelerator characterizing the GRB, i.e., the optically thick phase, while the third parameter is inherent to the environment surrounding the GRB which gives rise, by colliding with the baryonic fireshell, to the prompt radiation phase.

For the observational properties of a relativistically expanding fireshell model, a crucial concept has been the introduction of the EQui-Temporal Surfaces (EQTS). Here too our model differs from those in the literature by having deriving an analytic expression of the EQTS obtained from the solutions to the equations of motion [85, 95].

Details of the P-GRB and GRB prompt radiation are given in [13]. Before closing is here appropriate to recall the fundamental diagram comparing and contrasting the P-GRB and the Prompt radiation see Fig. 13 characterizing in the fireshell model the difference between short and long GRBs as a function of the baryon load.

2. UNVEILING THE GRB-SN CONNECTION: THE SECOND PARADIGM

2.1. Introduction

Until 1998 the study and GRBs and Supernovae continued in parallel but disjoint. Conceptually I had adopted the above mentioned first paradigm: that Supernovae originated from the formation of a neutron star and that GRB were generated by the formation of a Black Hole. Something totally unexpected happened on April 25, 1998: the occurrence of GRB 980425 and the simultaneous observation of SN 1998bw, see [19–21]. This coincidence have become extremely common for all long GRBs at cosmological red shift less then one.

While the collapsar and other groups started to attempt hybrid models of neutrons tars and Black

Holes Supernovae creating Black Holes and similar ideas I stay fixed to the above first paradigm and introduced a new "second paradigm":

Second paradigm

- *All long GRBs are necessarily associated to* ***SN Ic*** *and are components of a* ***"Cosmic Matrix."***
- *They originate from a massive binary system, which evlolves through a binary X-ray source, and finally leads to a binary system composed of a* ***FeCO*** *core* $> 2.8 M_\odot$ *and a* ***NS*** *companion separated by* $b_{crit} \sim 10^{11}$ *cm. For* $b < b_{crit}$ *hypercritical accretion of the SN ejecta onto the NS leads to a BH formation and to the consequent emission of a GRB. For* $b > b_{crit}$ *no* ***BH*** *is formed.*
- *For* $b < b_{crit}$ *a Binary-Driven Hypernova (****BdHN****) occurs characterized by:* ***Episode 1*** *the hypercritical accretion,* ***Episode 2*** *the GRB,* ***Episode 3*** *the universal behavior, and* ***Episode 4*** *the optical SN observed. For* $b > b_{crit}$ *only* ***Episode 1*** *and* ***Episode 4*** *exist, and an* ***X-Ray Flash*** *occurs*."

Evolving on an earlier formulation [96] the paradigm has lately evolved, see Fig. 15. All these theoretical works and their observational feed back have lead recently to the Binary driven Hypernova model (BdHN) [97, 98]. Contrary to the collapsar model that envisions a single object and a single event characterizing the GRBs Supernova association, the IGC paradigm assumes as a progenitor a binary system formed by an evolved FeCo core and a tightly bound neutron star binary companion, see Fig. 14. What was previously conceived for the GRB as a single ultra-relativistic event characterized by a jetted emission appears to be a much more complex and rich system composed generally of four different Episodes distinctively different in their astrophysical nature and with very specific signatures in their spectral and time varying luminosity emissions in selected wavelengths.

In conclusion, the IGC binary scenario applied here to the specific case of GRB 090618 naturally leads to understanding the energetics and the temporal coincidence of SN and GRBs, as well as their astrophysical scenario and makes the correlation of GRBs and SNe a direct consequence of the binary nature of the progenitor. In summary, we present in Figs. 16, 17 the full interpretation of GRB 090618 observations as the four different Episodes of the IGC paradigm.

Let us identify these four events in GRB 090618 the prototype of this most energetic family of GRBs, with an $E_{\rm iso}$ energy larger than 10^{52} erg, associated with Supernovae.

I will describe a few key moments in the recent evolution of our understanding of this system which is very unique within physics and astrophysics. Some twenty additional examples of such a GRBs associated to Supernovae have been identified by our group leading to the concept of Binary driven Hypernovae or BdHN .

2.2. The Case of GRB 090618

GRB 090618 represents the prototype of a class of energetic ($10^{52} \leq E_{\rm iso} \leq 10^{55}$ erg) GRBs, characterized by the presence of a supernova observed 10 $(1 + z)$ days after the trigger time, and the observation of four distinct emission episodes in their Gev emission, hard X-ray light curve, soft X ray and optical (see details in [39]). It was discovered by the Swift satellite [102]. The BAT light curve shows a multi-peak structure, whose total estimated duration is ∼320 s and whose T_{90} duration in the 15–350 keV range was 113 s [103]. The first 50 s of the light curve shows a smooth decay trend followed by a spiky emission, with three prominent peaks at 62, 80, and 112 s after the trigger time, respectively, and each have the typical appearance of a FRED pulse [104]. The XRT observations started 125 s after the BAT trigger time and lasted ∼25.6 ks [105] and reported an initially bright uncatalogued source, identified as the afterglow of GRB 090618. Its early decay is very

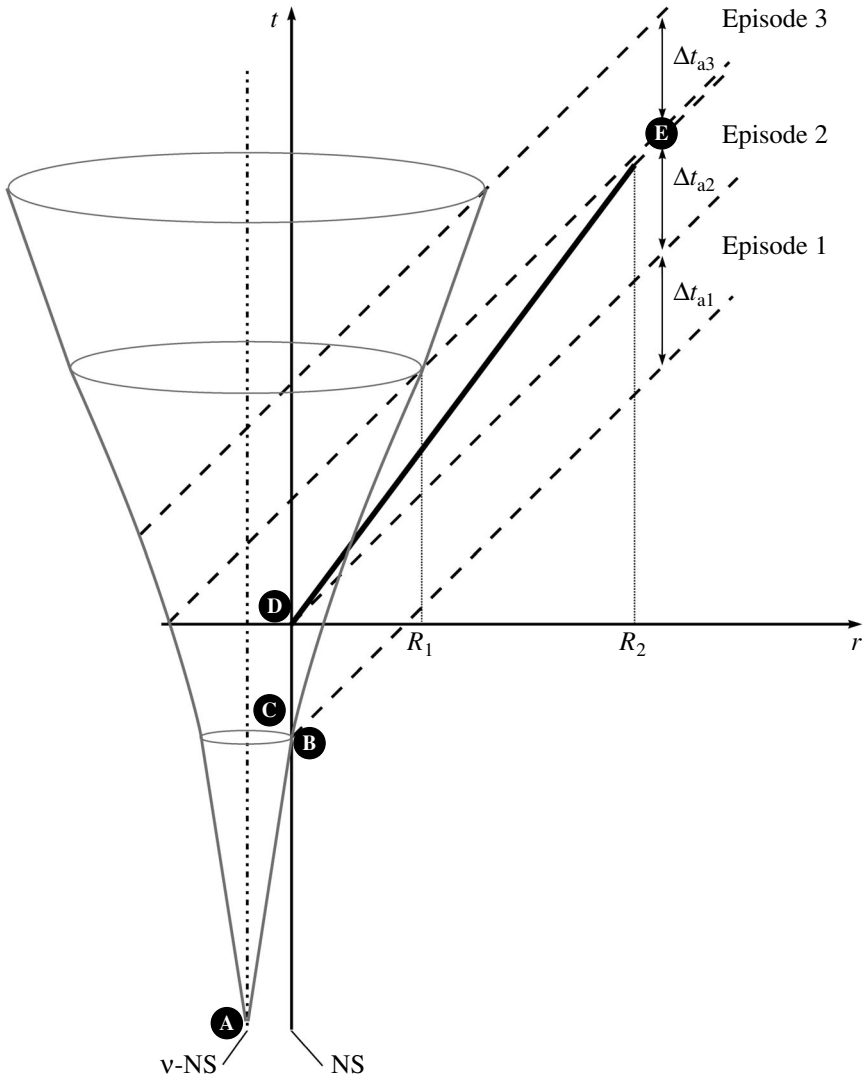

Fig. 15. IGC space-time diagram (not in scale), from [97]. Episode 1 corresponds to the onset of the FeCO core SN explosion, creating a new-NS (ν-NS, see A). Part of the SN ejecta triggers an accretion process onto the NS companion (see B and [40, 99]), and a prolonged interaction between the ν-NS and the NS binary companion occurs (see C). This leads to a spectrum with an expanding thermal component plus an extra power law (see Fig. 16 in [39]). Episode 2 occurs when the companion NS reaches its critical mass and collapses to a black hole (BH), emitting the GRB (D) with Lorentz factors $\Gamma \approx 10^2 - 10^3$ (for details, see e.g. [39, 48]). Episode 3, observed in the X-rays, shows very precise behavior consisting of a steep decay, starting at the end point of the prompt emission (see E), and then a plateau phase, followed by a late constant power-law decay (see [39, 100]). It is illustrated the relativistic motion of Episode 2 ($\Gamma \approx 500$, thick line) and the non-relativistic Episode 1 ($\Gamma \approx 1$) and Episode 3 ($\Gamma \approx 2$). Emissions from different radii, R_1 ($\sim 10^{13}$ cm) and R_2 ($\sim 10^{16} - 10^{17}$ cm), contribute to the transition point (E). Clearly, the X-ray luminosity originates in the SN remnant or in the newly-born BH, but not in the GRB.

steep, ending at 310 s after the trigger time, when it starts a shallower phase, the plateau. Then the light curve breaks into a steeper late phase. GRB 090618 was observed also by the Gamma-ray Burst Monitor (GBM) on board the Fermi satellite [106]. From a first analysis, the time-integrated spectrum, $(t_0, t_0 + 140)$ s in the 8–1000 keV range, was fit by a Band [107] spectral model, with a peak energy $E_{\rm peak} = 155.5$ keV, $\alpha = -1.26$ and $\beta = -2.50$ [108], but with strong spectral variations within the considered time interval. The redshift of the source is $z = 0.54$ and it was determined thanks to the identification of the MgII, MgI, and FeII absorption lines using the KAST spectrograph mounted at the 3 m Shane telescope at the Lick observatory [109]. Given the redshift and the distance of the source, we computed the emitted isotropic energy in the 8–10 000 keV energy range, with the Schaefer formula [110]: using the fluence in the (8–1000 keV) as observed by Fermi-GBM, $S_{\rm obs} = 2.7 \times 10^{-4}$ [108], and the

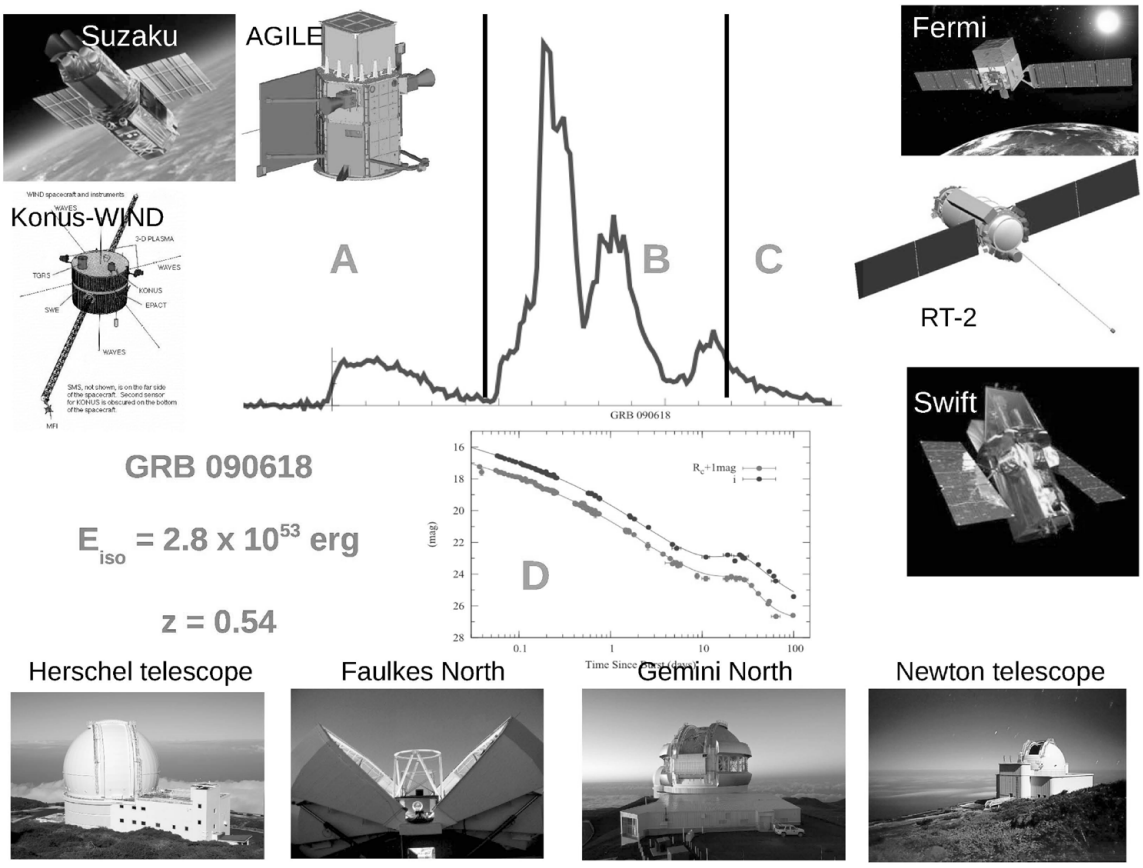

Fig. 16. GRB 090618 observations as the the four different Episodes implied by the IGC paradigm: (A) Episode 1, (B) Episode 2, (C) Episode 3, and (D) Episode 4 (i.e., the optical observations of the associted SN). Above are the satellites that participated in the observations: (in clockwise order) Fermi/GBM (8–1000 keV), Coronas-Photon/RT-2 (15–1000 keV), Swift/BAT (15–150 keV), Swift/XRT (0.3–10 keV), Swift/UVOT (optical band), AGILE/Super-AGILE (18–60 keV), AGILE/MCAL (350–10^5 keV), Suzaku/WAM (50–5000 keV), Konus/WIND (20–2000 keV). Below are the ground based observatories that participated in the optical observations. Details in [39, 40, 101].

ΛCDM (Λ Cold Dark Matter) cosmological standard model $H_0 = 70$ km/s/Mpc, $\Omega_m = 0.27$, $\Omega_\Lambda = 0.73$, we obtain for the emitted isotropic energy the value of $E_{\rm iso} = 2.90 \times 10^{53}$ erg. This GRB was observed also by Konus-WIND [111], Suzaku-WAM [112], and by the AGILE satellite [113], which detected emission in the (18–60) keV and in the MCAL instrument, operating at energies greater than 350 keV, but it did not observe high-energy photons above 30 MeV. GRB 090618 was the first GRB observed by the Indian payloads RT-2 on board the Russian satellite CORONAS-PHOTON [114–116]. Thanks to the complete data coverage of the optical afterglow of GRB 090618, the presence of a supernova underlying the emission of its optical afterglow was reported [117]. The evidence of a supernova emission came from the presence of several bumps in the light curve and by the change in $R_c - i$ color index over time: in the early phases, the blue color is dominant, typical of the GRB afterglow, but then the color index increases, suggesting a core-collapse SN. At late times, the contribution from the host galaxy was dominant. We have analyzed, with L. Izzo and other ICRANet researchers and Ph.D. students, GRB 090618, considering the BAT and XRT data of the Swift satellite together with the Fermi-GBM and RT2 data of the Coronas-PHOTON satellite (see Fig. 16). The data reduction was made with the Heasoft v6.10 packages[1] for BAT and XRT, and the Fermi-Science tools for GBM. The details of the data reduction and analysis are given in [39].

2.3. The Emission Process in Episode 1

2.3.1. The time-resolved spectra and temperature variation. A significant outcome of the multi-year work of Felix Ryde and his collaborators [118] has been the identification of a the thermal plus power-law features observed in time-limited intervals

[1] http://heasarc.gsfc.nasa.gov/lheasoft/

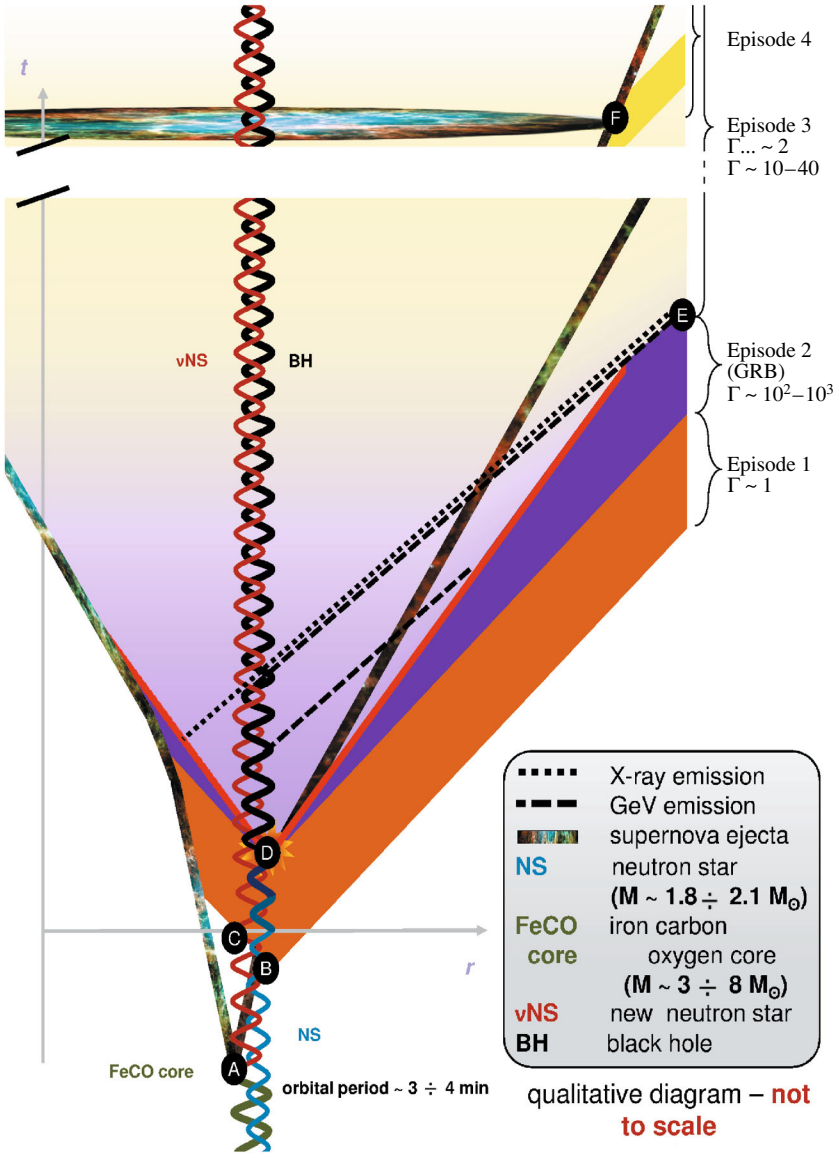

Fig. 17. IGC space-time diagram (not in scale) illustrates 4 episodes of IGC paradigm: the non-relativistic Episode 1 ($\Gamma \simeq 1$), the relativistic motion of Episode 2 ($\Gamma \simeq 10^2$–10^3), the mildly relativistic Episode 3 ($\Gamma \simeq 2$), and non-relativistic Episode 4 ($\Gamma \simeq 1$). Initially there is a binary system composed by a massive star (yellow thick line) and a neutron star (blue line). The massive star evolves and explodes as a SN at point A, forms a νNS (red line). The companion NS accretes the supernova ejecta starting from point B, interacts with the ν-NS starting from point C, and collapses into a black hole (black line) at point D, this period from point B to point D we define as Episode 1. Point D is the starting of Episode 2, due to the collision of GRB outflow and interstellar filaments. At point E, Episode 2 ends and Episode 3 starts, Episode 3 lasts till the optical signal of supernova emerges at point F, where the Episode 4 starts. (*Credit to M.Enderli on drawing this visualized space–time diagram.*)

in selected BATSE GRBs. Similar features have also been observed in the data acquired by the Fermi satellite [118, 119]. These emission have been shown to present a thermal plus power-law(s) feature, with a temperature changing in time following a precise power-law behavior. Our aim has been to see if the first 50 seconds of emission of GRB 090618 conform to this feature. We made a detailed time-resolved analysis, considering different time bin durations to obtain good statistics in the spectra and to take into account the sub-structures in the light curve. We then used two different spectral models to fit the observed data, a classical Band spectrum [107], and a blackbody with a power-law component. To obtain more accurate constraints on the spectral parameters, we made a joint fit considering the observations from

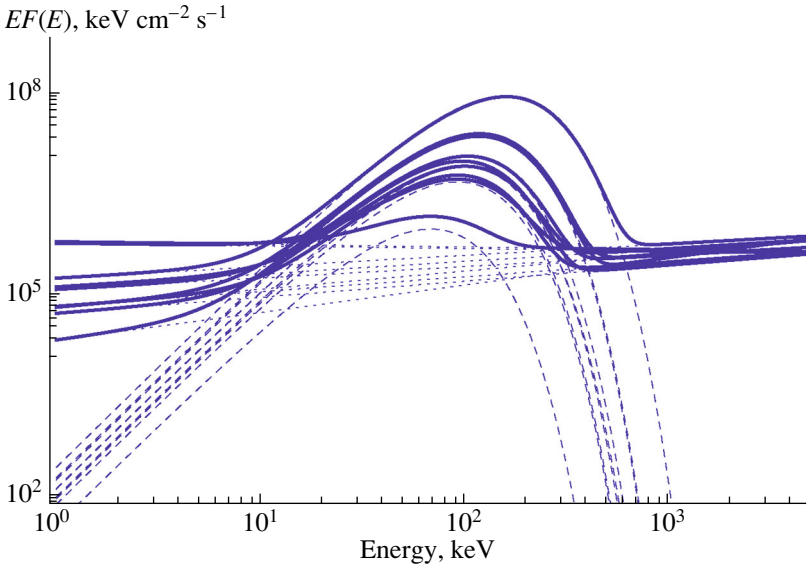

Fig. 18. Evolution of the BB + powerlaw spectral model in the $\nu F(\nu)$ spectrum of the first emission of GRB 090618. It shows the cooling with time of the blackbody and associated nonthermal components. We only plot the fitting functions for clarity. From [39].

both the n4 NaI and the b0 BGO detectors, covering a wider energy range in this way, from 8 keV to 40 MeV. To avoid some bias from low-photon statistics, we considered an energy upper limit of the value of 10 MeV. Our analysis is summarized in Figs. 18, 19 and 20.

2.3.2. The power-law decay of the black body temperature. Particularly interesting is the clear evolution in the time-resolved spectra, which corresponds to the blackbody and power-law component, see Fig. 18. In particular the kT parameter of the blackbody shows a strong decay, with a temporal behavior well-described by a double broken power-law function, see the upper panel in Fig. 19. From a fitting procedure we find that the best fit (R^2-statistic = 0.992) for the two decay indexes for the temperature variation are $a_{kT} = -0.33 \pm 0.07$ and $b_{kT} = -0.57 \pm 0.11$. In [80] an average value for these parameters on a set of 49 GRBs is given: $\langle a_{kT} \rangle = -0.07 \pm 0.19$ and $\langle b_{kT} \rangle = -0.68 \pm 0.24$. The results presented in Figs. 18 and 19, point to a rapid cooling of the thermal emission with time of the first episode. The evolution of the corresponding power-law spectral component also appears to be strictly related to the change of the temperature kT. The power-law γ index falls, or softens, with temperature, see Fig. 18. An interesting feature appears to occur at the transition of the two power-laws describing the observed decrease of the temperature.

2.3.3. The radius of the emitting region. We turn now to estimate an additional crucial parameter for identifying the nature of the blackbody component: the radius of the emitter $r_{\rm em}$. We proved that the first episode is not part of a GRB. We can therefore provide the estimate of the emitter radius from nonrelativistic considerations, just corrected for the cosmological redshift z. In fact we find that the temperature of the emitter $T_{\rm em} = T_{\rm obs}(1+z)$, and that the luminosity of the emitter, due to the blackbody emission, is

$$L = 4\pi r_{\rm em}^2 \sigma T_{\rm em}^4 = 4\pi r_{\rm em}^2 \sigma T_{\rm obs}^4 (1+z)^4, \quad (2)$$

where $r_{\rm em}$ is the emitter radius and σ is the Stefan–Boltzmann constant. From the luminosity distance definition, we also have that the observed flux $\phi_{\rm obs}$ is given by

$$\phi_{\rm obs} = \frac{L}{4\pi D^2} = \frac{r_{\rm em}^2 \sigma T_{\rm obs}^4 (1+z)^4}{D^2}. \quad (3)$$

We then obtain

$$r_{\rm em} = \left(\frac{\phi_{\rm obs}}{\sigma T_{ob}^4}\right)^{1/2} \frac{D}{(1+z)^2}. \quad (4)$$

The above radius differs from the radius r_{ph} given in Eq. (1) of [80], which was also clearly obtained by interpreting the early evolution of GRB 970828 as belonging to the photospheric emission of a GRB and assuming a relativistic expansion with a Lorentz gamma factor Γ

$$r_{ph} = \hat{\mathcal{R}} D \left(\frac{\Gamma}{(1.06)(1+z)^2}\right), \quad (5)$$

where $\hat{\mathcal{R}} = \left(\phi_{\rm obs}/(\sigma T_{ob}^4)\right)^{1/2}$ and the prefactor 1.06 arises from the dependence of r_{ph} on the angle of

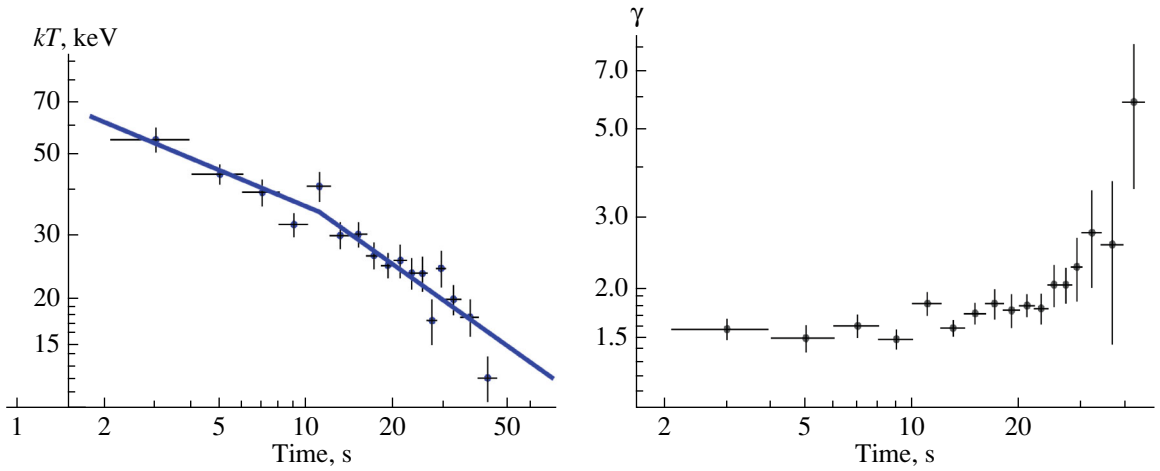

Fig. 19. Evolution of the observed temperature kT of the blackbody component and the corresponding evolution of the power-law photon index. The blue line in the upper panel corresponds to the fit of the time evolution of the temperature with a broken power-law function. It shows a break time t_b around 11 s after the trigger time, as obtained from the fitting procedure. From [39].

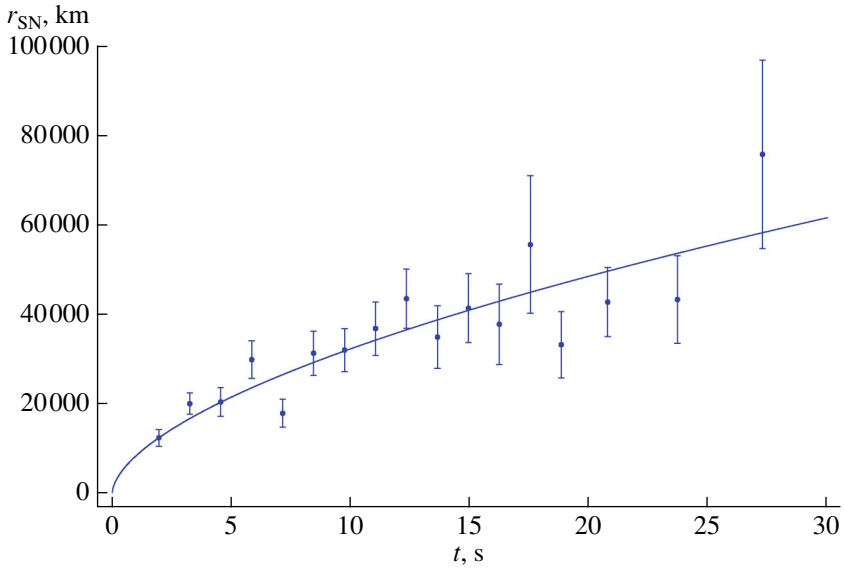

Fig. 20. Evolution of the Episode 1 emitter radius given by Eq. (4). From [39].

the line of sight [120]. Typical values of r_{ph} are at least two orders of magnitude higher than our radius $r_{\rm em}$. Assuming a standard cosmological model ($H_0 = 70$ km/s/Mpc, $\Omega_m = 0.27$ and $\Omega_\Lambda = 0.73$) for estimating the luminosity distance D, and using the values for the observed flux $\phi_{\rm obs}$ and the temperature $kT_{\rm obs}$, we give in Fig. 20 the evolution of the surface radius that emits the blackbody $r_{\rm em}$ as a function of time. Assuming an exponential evolution with time t^δ of the radius in the comoving frame, we obtain the value $\delta = 0.59 \pm 0.11$ from a fitting procedure, which is well compatible with $\delta = 0.5$. We also notice a steeper behavior for the variation of the radius with time corresponding to the first 10 s, which corresponds to the emission before the break of the double power-law behavior of the temperature. We estimate an average velocity of $\bar{v} = 4067 \pm 918$ km/s, $R^2 = 0.91$ in these first 10 s of emission. In Episode 1 the observations lead to a core of an initial radius of ∼12 000 km expanding in the early phase with a higher initial velocity of ∼4000 km/s. The effective Lorentz Γ factor is very low, $\Gamma - 1 \sim 10^{-5}$. I proposed

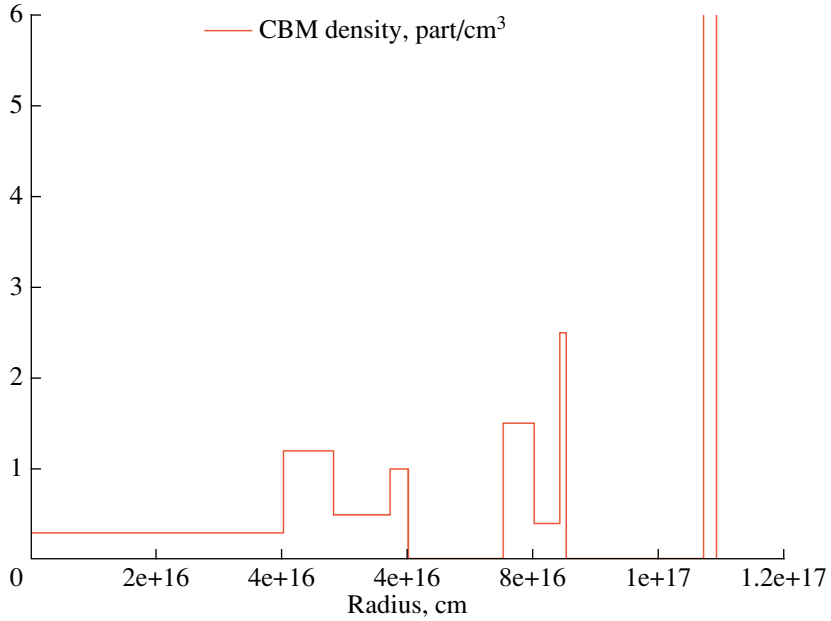

Fig. 21. Radial CBM density distribution for GRB 090618. The characteristic masses of each cloud are on the order of $\sim 10^{22-24}$ g and 10^{16} cm in radii. From [39].

to identify this first episode as the early phases of the accretion on the companion NSr of the SN ejects in the IGC scenario. later confirmed by the simulation in Freyer et al. presented in the next paragraphs.

2.4. The Emission Process in Episode 2

2.4.1. The identification of the P-GRB. We have proceeded to the analysis of the data between 50 and 150 s after the trigger time as a canonical GRB in the fireshell scenario, namely Episode 2 [101]. We proceed to identify the P-GRB within the emission between 50 and 59 s, since we find a blackbody signature in this early second-episode emission. Considerations based on the time variability of the thermal component bring us to conclude that the first 4 s of this time interval to due to the P-GRB emission. The corresponding spectrum (8–440 keV) is well fit ($\tilde{\chi}^2 = 1.15$) with a blackbody of a temperature $kT = 29.22 \pm 2.21$ keV (norm $= 3.51 \pm 0.49$), and an extra power-law component with photon index $\gamma = 1.85 \pm 0.06$, (norm $= 46.25 \pm 10.21$). The fit with the Band model is also acceptable ($\tilde{\chi}^2 = 1.25$), which gives a low-energy power-law index $\alpha = -1.22 \pm 0.08$, a high-energy index $\beta = -2.32 \pm 0.21$ and a break energy $E_0 = 193.2 \pm 50.8$. In view of the theoretical understanding of the thermal component in the P-GRB (see Section 3.2), we focus below on the blackbody + power-law spectral model. The isotropic energy of the second episode is $E_{\rm iso} = (2.49 \pm 0.02) \times 10^{53}$ erg. The simulation within the fireshell scenario is made assuming $E_{\rm tot}^{e^+e^-} \equiv E_{\rm iso}$. From the observed temperature, we can then derive the corresponding value of the baryon load. The observed temperature of the blackbody component is $kT = 29.22 \pm 2.21$, so that we can determine a value of the baryon load of $B = (1.98 \pm 0.15) \times 10^{-3}$, and deduce the energy of the P-GRB as a fraction of the total $E_{\rm tot}^{e^+e^-}$. We therefore obtain a value of the P-GRB energy of $4.33^{+0.25}_{-0.28} \times 10^{51}$ erg. Now we can derive the radius of the transparency condition, to occur at $r_{\rm tr} = 1.46 \times 10^{14}$ cm. We derive the bulk Lorentz factor of $\Gamma_{th} = 495$. We compare this value with the energy measured only in the blackbody component of $E_{BB} = 9.24^{+0.50}_{-0.58} \times 10^{50}$ erg, and with the energy in the blackbody plus the power-law component of $E_{BB+po} = 5.43^{+0.07}_{-0.11} \times 10^{51}$ erg, and verify that the theoretical value is in between these observed energies. We have found this result to be quite satisfactory: it represents the first attempt to relate the GRB properties to the details of the BH responsible for the overall GRB energetics. The above theoretical estimates were based on a nonrotating BH of 10 $M_\odot$, a total energy of $E_{\rm tot}^{e^+e^-} = 2.49 \times 10^{53}$ erg and a mean temperature of the initial e^+e^- plasma of 2.4 MeV, derived from the expression for the dyadosphere radius, Eq. (1).

2.4.2. The refinement of the P-GRB nature. Standing the excellent results obtained in the e^+e^- spectra and the dynamics the refinement of the di-

Table 1. Final results of the simulation of GRB 090618 in the fireshell scenario. From [39]

Parameter	Value
$E_{\rm tot}^{e^+e^-}$	$(2.49 \pm 0.02) \times 10^{53}$ erg
B	$(1.98 \pm 0.15) \times 10^{-3}$
Γ_0	495 ± 40
kT_{th}	29.22 ± 2.21 keV
$E_{P\text{-}GRB,th}$	$(4.33 \pm 0.28) \times 10^{51}$ erg
$\langle n \rangle$	0.6 part/cm^3
$\langle \delta n/n \rangle$	2 part/cm^3

Table 2. Physical properties of the three clouds surrounding the burst site: the distance from the burst site (column 2), the radius r of the cloud (column 3), the particle density ρ (column 4), and the mass M (the last column). From [39]

Cloud	Distance (cm)	r (cm)	ρ (#/cm^3)	M (g)
First	4.0×10^{16}	1×10^{16}	1	2.5×10^{24}
Second	7.4×10^{16}	5×10^{15}	1	3.1×10^{23}
Third	1.1×10^{17}	2×10^{15}	4	2.0×10^{22}

rect comparison between theory and observations will have to address a variety of fundamental problems such as 1) the possible effect of rotation of the BH, leading to a more complex dyadotorus structure [22], 2) an analysis of the general relativistic, electrodynamical, strong interaction descriptions of the gravitational core collapse leading to BH formation [82, 121, 122], 3) a possible role of hypercritical accretion process in creating the electron-positron plasma out of neutrino-antineutrino annihilalation [24, 37, 123]. All these processes could alternatively lead to the dyadosphere near the Kerr–Newmann black hole with an efficiency (42 percent) similar to the electrodynamical case (50 percent).

2.4.3. The prompt emission and the CBM cloud structure. The prompt emission starts at the above given radius of the transparency, with an initial value of the Lorentz Γ factor of $\Gamma_0 = 495$. To simulate the extended-afterglow emission, we need to determine the radial distribution of the CBM around the burst site, which we assume for simplicity to be spherically symmetric, from which we infer a characteristic size of $\Delta R = 10^{15}$–10^{16} cm. We already described above how the simulation of the spectra and of the observed multi-band light curves have to be performed together and need to be jointly optimized, leading to the determination of the fundamental parameters characterizing the CBM medium [124]. This radial distribution is shown in Fig. 21 and is characterized by a mean value of $\langle n \rangle = 0.6$ part/cm^3 and an average density contrast with a $\langle \delta n/n \rangle \approx 2$, see Fig. 21 and Tables 1 and 2. The data up to 8.5×10^{16} cm are simulated with a value for the filling factor $\mathcal{R} = 3 \times 10^{-9}$, while the data from this value on with $\mathcal{R} = 9 \times 10^{-9}$. From the radial distribution of the CBM density, and considering the $1/\Gamma$ effect on the fireshell visible area, we found that the CBM clumps causing the spikes in the extended-afterglow emission have masses on the order of 10^{22}–10^{24} g. The value of the α parameter was found to be -1.8 along the total duration of the GRB. In Fig. 22 we show the simulated light curve (8–1000 keV) of the GRB and the corresponding spectrum, using the spectral model described in [84, 125]. The Episode 2, lasting from 50 to 151 s, agrees with a canonical GRB in the fireshell scenario.

2.5. The Emission Process of Episode 3

2.5.1. The late X-ray emission observed by swift/XRT. I turn now to the most important feature which has appeared in the analysis of Episode 3 of GRB 090618. The presence of a steep decay, followed by a plateau and a power law steep decay, see Fig. 23. This feature unexpectedly has become a common feature of all GRBs with energy larger then $10 + 52$ erg and even more striking all the Xray emissions at late time, when computed in the rest frame of the source they overlap, see Fig. 24. This occurrence has become a most powerful method to estimate the cosmological redshift of the source, where not directly observed. We have focused our attention on the analysis of all the available XRT data of these sources [41]. Characteristically, XRT follow-up starts only about 100 seconds after the BAT trigger (typical repointing time of Swift after the BAT trigger). Since the behavior was similar in all the sources, we have performed an analysis to compare the XRT luminosity light curve L_{rf} for the six GRBs with measured redshift z in the common rest frame energy range 0.3–10 keV. To perform this computation, the first step is to convert the observed XRT flux $f_{\rm obs}$ to the one in the 0.3–10 keV rest frame energy range. In the detector frame, the 0.3–10 keV rest frame energy range becomes $[0.3/(1+z)]$–$[10/(1+z)]$ keV where z is the redshift of the GRB. We assume a simple power-law function as the best-fit for the spectral energy distribution of the XRT data:[2]

$$\frac{dN}{dAdtdE} \propto E^{-\gamma}. \qquad (6)$$

[2] http://www.swift.ac.uk/

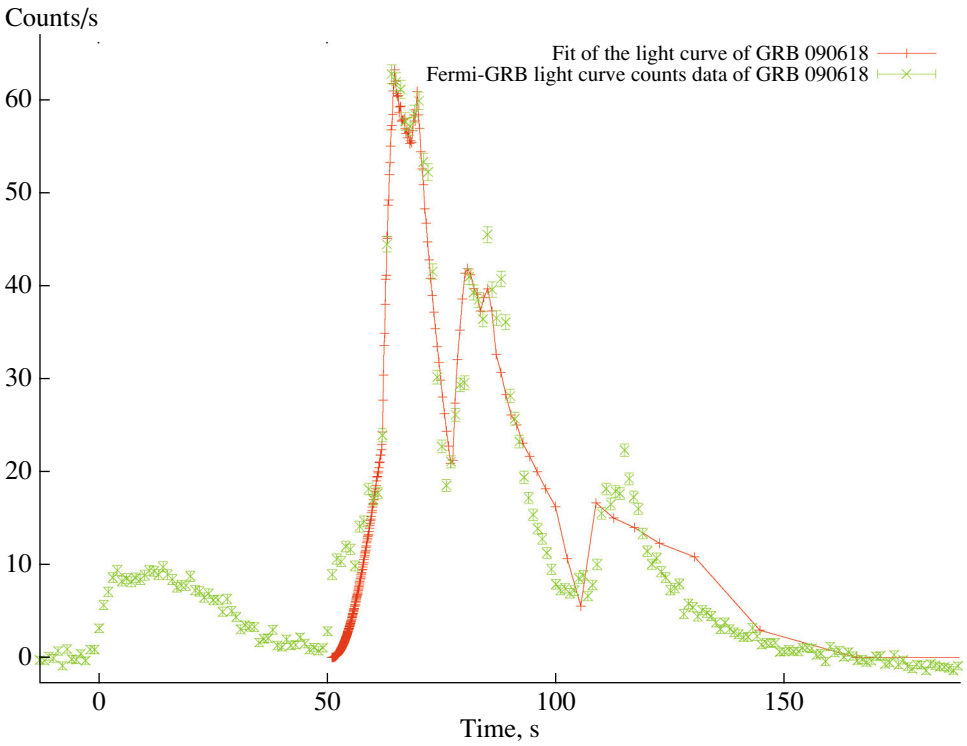

Fig. 22. Simulated light curve and time integrated ($t_0 + 58$, $t_0 + 150$ s) spectrum (8–440 keV) of the extended-afterglow of GRB 090618. From [39].

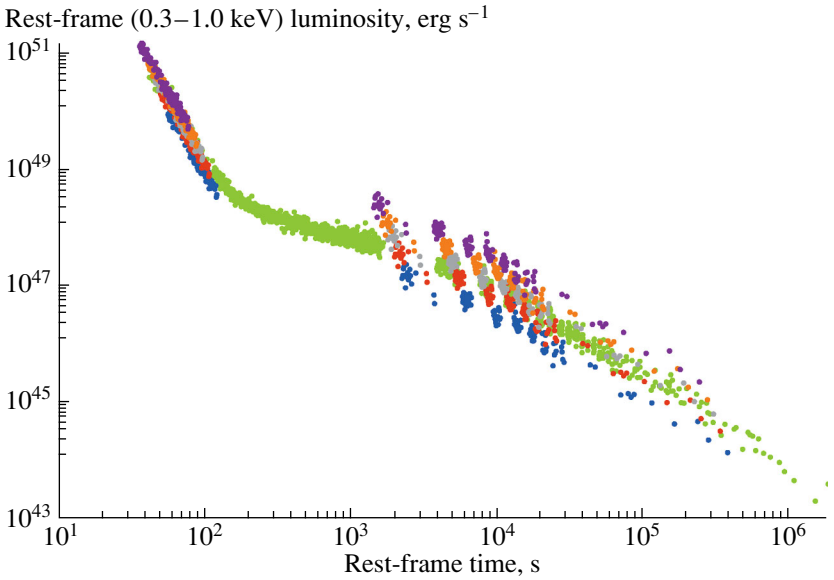

Fig. 23. In green we show the rest frame X-ray luminosity light curve of GRB 090618 in the 0.3–10 keV energy range in comparison with the one of GRB 101023 (left) and GRB 110709B (right), computed for different hypothetical redshifts: respectively, from blue to purple: $z = 0.6, 0.8, 1.0, 1.2, 1.5$ (left) and $z = 0.4, 0.6, 0.8, 1.0, 1.2$ (right). The overlapping at late time of the two X-ray luminosity light curves is obtained for a redshift of $z = 0.9$ (left) and $z = 0.75$ (right). For further details see [100, 126].

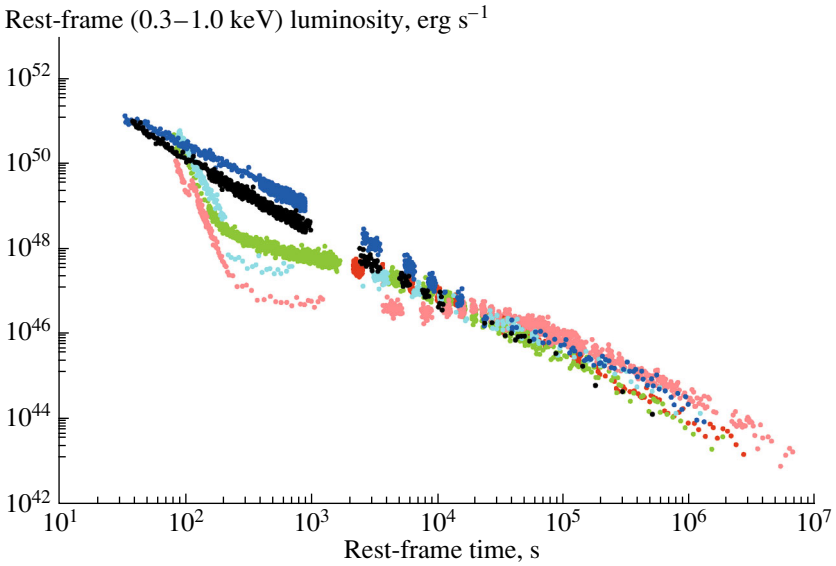

Fig. 24. The X-ray luminosity light curves of the six GRBs with measured redshift in the 0.3–10 keV rest frame energy range: in pink GRB 060729, $z = 0.54$; in black GRB 061007, $z = 1.261$; in blue GRB 080319B, $z = 0.937$; in green GRB 090618, $z = 0.54$, in red GRB 091127, $z = 0.49$, in cyan GRB 111228, $z = 0.713$. From [41].

We can then write the flux light curve f_{rf} in the 0.3–10 keV rest frame energy range as:

$$f_{rf} = f_{\rm obs} \frac{\int_{\frac{0.3\ \rm keV}{1+z}}^{\frac{10\ \rm keV}{1+z}} E^{-\gamma} dE}{\int_{0.3\ \rm keV}^{10\ \rm keV} E^{-\gamma} dE} = f_{\rm obs}(1+z)^{\gamma-1}. \quad (7)$$

Then, we have to multiply f_{rf} by the luminosity distance to get L_{rf}:

$$L_{rf} = 4\pi d_l^2(z) f_{rf}, \quad (8)$$

where we assume a standard cosmological model ΛCDM with $\Omega_m = 0.27$ and $\Omega_\Lambda = 0.73$. Clearly, this luminosity must be plotted as a function of the rest frame time t_{rf}, namely:

$$t_{rf} = \frac{t_{\rm obs}}{1+z}. \quad (9)$$

2.5.2. "The golden sample." The X-ray luminosity light curves of the six GRBs with measured redshift in the 0.3–10 keV rest frame energy band are plotted together in Fig. 24 and Table 3. What is most striking is that these six GRBs, with redshift in the range 0.49–1.261, show a remarkably common behavior of the late X-ray afterglow luminosity light curves (Episode 3) despite that their prompt emissions (Episode 1 and 2) are very different and that their energetics spans more than two orders of magnitude, see Table 3. Such a common behavior starts between 10^4–10^5 s after the trigger and continues up to when the emission falls below the XRT threshold. This standard behavior of Episode 3 represents strong evidence of very low or even the absence of beaming in this particular phase of the X-ray afterglow emission process. I proposed that this late time X-ray emission in Episode 3 is related to the process of the SN explosion within the IGC scenario, possibly emitted by the newly born NS and BH and by the supernovae ejecta shocked by the GRB, and not by the GRB itself.

2.5.3. Episode 3 as a standard candle. As an example, we present in Fig. 23 the rest frame X-ray luminosity (0.3–10 keV) light curve of GRB 090618 (considered as a prototype for the common behavior shown in Fig. 24) with the rest frame

Table 3. The GRB sample considered in this work. The redshifts of GRB 101023 and GRB 110709B, which are marked by an asterisk, were deduced theoretically by using the method outlined in [100] and the corresponding isotropic energy computed by assuming these redshifts. From [41]

GRB	z	$E_{\rm iso}$ (erg)
GRB 060729	0.54	1.6×10^{52}
GRB 061007	1.261	1.2×10^{54}
GRB 080319B	0.937	1.4×10^{54}
GRB 090618	0.54	2.7×10^{53}
GRB 091127	0.49	1.4×10^{52}
GRB 111228	0.713	2.3×10^{52}
GRB 101023	0.9*	1.3×10^{53}
GRB 110709B	0.75*	2.72×10^{53}

X-ray luminosity light curves of GRB 110709B estimated for selected values of its redshifts, $z = 0.4, 0.6, 0.8, 1.0, 1.2$, and similarly the correspondent analysis for GRB 101023 for selected values of the redshift, $z = 0.6, 0.8, 1.0, 1.2, 1.5$. We then find, with A.V. Penacchioni and other ICRANet researchers and Ph.D. students, that GRB 101023 should have been located at $z \sim 0.9$ and GRB 110709B at $z \sim 0.75$. These redshift estimations are within the range expected using the Amati relation as shown in [100, 126]. This is an important independent confirmation of validity for this new redshift estimator we propose for the family of IGC GRB-SN systems. It should be stressed, however, that the determination of the redshift is done assuming the validity of the standard ΛCDM cosmological model for sources with redshift in the range $z = 0.49-1.216$. We are currently testing the validity of this assumption for sources at larger cosmological redshifts.

3. THE GRB-SN AND THE IGC: THE SECOND PARADIGM

3.1. Induced Gravitational Collapse of a NS to a BH by a Type Ib/c SN

The systematic and spectroscopic analysis of GRB-SN events, following the pioneering discovery of the temporal coincidence of GRB 980425 [19] and SN 1998bw [21], has revealed evidence for the association of other nearby GRBs with Type Ib/c SNe (see [127] for a recent review of all the GRB-SN systems). It has also been clearly understood that SN Ib/c lack Hydrogen (H) and Helium (He) in their spectra, and the most likely explanation is that the SN progenitor star is in a binary system with a compact companion, a neutron star (see e.g. [128–130], for details). In the current literature there has been an attempt to explain both the SN and the GRB as two aspects of the same astrophysical phenomenon: the collapsar model. Hence, GRBs have been assumed to originate from a specially violent SN process, a hypernova or a collapsar (see e.g. [131] and references therein). Both of these possibilities imply a very dense and strong wind-like CBM structure. Such a dense medium appears to be in contrast with the CBM density found in most GRBs within our fireshell model (see e.g. Fig. 10 in [40]). In fact, the average CBM density, inferred from the analysis of the afterglow, has been shown to be in most of the cases of the order of 1 particle cm^{-3} (see e.g. [49]). The only significant contribution to the baryonic matter component in the GRB process is the one represented by the baryon load [33]. In a GRB, the electron-positron plasma, loaded with a certain amount of baryonic matter, is expected to expand at ultra-relativistic velocities with Lorentz factors $\Gamma \gtrsim 100$ [86, 132, 133]. Such an ultra-relativistic expansion can actually occur if the amount of baryonic matter, quantifiable through the baryon load parameter, does not exceed the critical value $B \sim 10^{-2}$ (see [33], for details). For $B > 10^{-2}$ the electron-positron plasma looses its laminar motion and the turbulence occurs, see Fig. 12.

In our approach, following the first paradigm, we have consistently assumed that the GRB has to originate from the gravitational collapse to a BH. The SN follows, instead, the complicated pattern of the final evolution of a massive star, possibly leading to a NS or to a complete explosion but never to a BH. There is a further general argument in favor of our explanation, namely the extremely different energetics of SNe and GRBs. While the SN energy range is $10^{49}-10^{51}$ erg, the GRBs are in a larger and wider range of energies $10^{49}-10^{54}$ erg. It is clear that in no way a GRB, being energetically dominant, can originate from the SN. We explain the temporal coincidence of the two phenomena, the SN explosion and the GRB, within the concept of *induced gravitational collapse* [96, 134]. In recent years we have outlined two different possible scenarios for the GRB-SN connection. In the first version [96], we have considered the possibility that GRBs may have caused the trigger of the SN event. For this scenario to occur, the companion star has to be in a very special phase of its thermonuclear evolution (see [96] for details). More recently, I have proposed in [124, 134, 135] a different possibility occurring at the final stages of the evolution of a close binary system: the explosion in such a system of a Ib/c SN leads to an accretion process onto the NS companion. The full space-time diagram is represented in Fig. 15. Again, in order for this process to occur, a very fine tuning must exist in the thermonuclear evolution of the SN core and in the circular orbit of the companion NS. The NS will reach the critical mass value, undergoing gravitational collapse to a BH. The process of gravitational collapse to a BH leads to the emission of the GRB (see Figs. 25 and 26). Here we evaluate the accretion rate onto the NS and give the explicit expression of the accreted mass as a function of the nature of the components and the binary parameters following [99]. The full space-time diagram is represented in Fig. 15.

3.2. The Accretion Process of the SN Ejecta onto the Companion NS

We turn now to the details of the recent work with Jorge Rueda [99] and collaborators, of the accretion process of the SN material onto the NS. In a spherically symmetric accretion process, the magnetospheric radius is [136]

$$R_m = \left(\frac{B^2 R^6}{\dot{M}\sqrt{2GM_{\rm NS}}} \right)^{2/7}, \qquad (10)$$

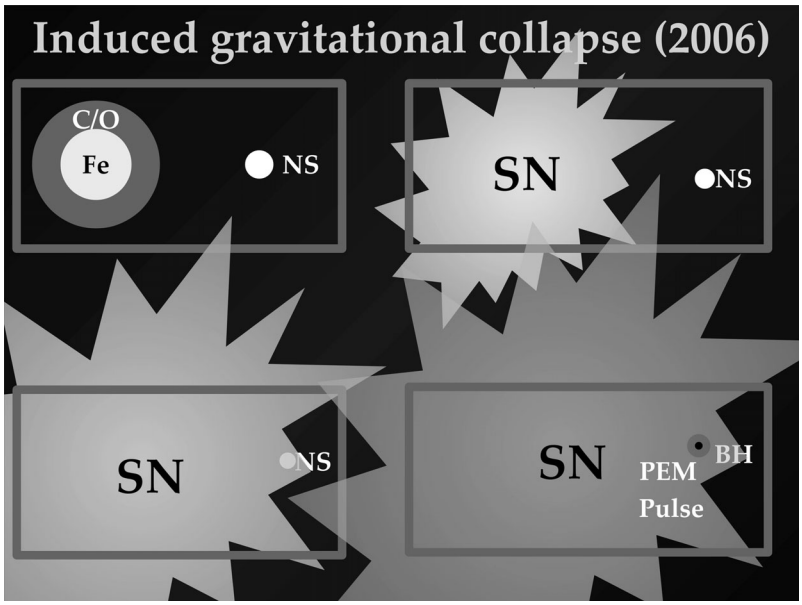

Fig. 25. Process of gravitational collapse to a BH induced by the type Ib/c SN on a companion NS in a close binary system. Figure reproduced from [134].

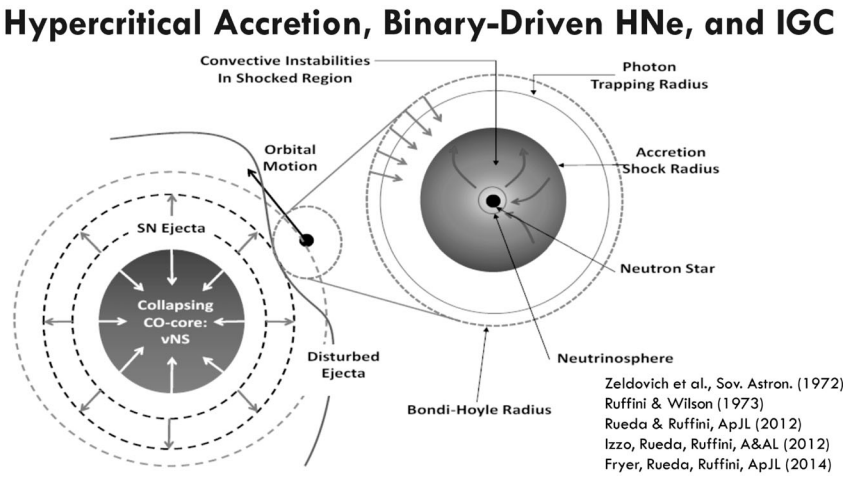

Fig. 26. Hypercritical accretion, binary-driven HNe, and IGC.

where B, $M_{\rm NS}$, R are the NS magnetic field, mass, radius, and $\dot{M} \equiv dM/dt$ is the mass-accretion rate onto the NS. It can be seen that for high accretion rates the influence of the magnetosphere will be negligible. The NS captures the material ejected from the core collapse of the companion star in a region delimited by the radius $R_{\rm cap}$ from the NS center

$$R_{\rm cap} = \frac{2GM_{\rm NS}}{v^2_{\rm rel,ej}}, \qquad (11)$$

where $M_{\rm NS}$ is the initial NS mass and $v_{\rm rel,ej}$ is the velocity of the ejecta relative to the orbital motion of the NS around the supernova progenitor star

$$v_{\rm rel,ej} = \sqrt{v^2_{\rm orb} + v^2_{\rm ej}}, \qquad (12)$$

with $v_{\rm ej}$ the ejecta velocity in the frame of the supernova progenitor star with mass $M_{\rm SN\text{-}prog}$ and $v_{\rm orb}$ is the orbital velocity of the NS, given by

$$v_{\rm orb} = \sqrt{\frac{G(M_{\rm SN\text{-}prog} + M_{\rm NS})}{a}}, \qquad (13)$$

where a is the binary separation, and thus the orbital period of the binary system is

$$P = \sqrt{\frac{4\pi^2 a^3}{G(M_{\rm SN\text{-}prog} + M_{\rm NS})}}. \quad (14)$$

The NS accretes the material that enters into its capture region defined by Eq. (11). The mass-accretion rate is given by [137]

$$\dot{M} = \xi\pi\rho_{\rm ej}R_{\rm cap}^2 v_{ej} = \xi\pi\rho_{ej}\frac{(2GM_{\rm NS})^2}{(v_{\rm orb}^2 + v_{ej}^2)^{3/2}}, \quad (15)$$

where the parameter ξ is lies in the range $1/2 \leq \xi \leq 1$, $\rho_{\rm ej}$ is the density of the accreted material, and in the last equality we have used Eqs. (11) and (12). The upper value $\xi = 1$ corresponds to the Hoyle-Lyttleton accretion rate [138]. The actual value of ξ depends on the properties of the medium in which the accretion process occurs, e.g., vacuum or wind. The velocity of the SN ejecta $v_{\rm ej}$ will be much larger than the sound speed c_s of the already existing material between the C + O star and the NS due to the prior mass transfer, namely, the Mach number of the SN ejecta will certainly satisfy $\mathcal{M} = v_{\rm ej}/c_s \gg 1$. Thus in practical calculations we can assume the value $\xi = 1$ in Eq. (15) and the relative velocity $v_{\rm rel,ej}$ of the SN ejecta with respect to the NS companion is given only by the NS orbital velocity and the ejecta velocity as given by Eq. (12). In Fig. 26 we have sketched the accreting process of the supernova ejected material onto the NS. The density of the ejected material can be assumed to decrease in time following the simple power-law [139]

$$\rho_{\rm ej} = \frac{3M_{\rm ej}}{4\pi r^3} = \frac{3M_{\rm ej}}{4\pi\sigma^3 t^{3n}}, \quad (16)$$

where without loss of generality we have assumed that the radius of the SN ejecta expands as $r_{\rm ej} = \sigma t^n$, with σ and n constants. Therefore the velocity of the ejecta obeys $v_{\rm ej} = nr_{\rm ej}/t$. Equation (15) can be integrated analitically and the accreted mass in a given time interval is given by [99]

$$\Delta M(t) = \int \dot{M}dt$$
$$= \pi(2GM_{\rm NS})^2\frac{3M_{\rm ej}}{4\pi n^3\sigma^6}\mathcal{F} + \text{constant}, \quad (17)$$

where

$$\mathcal{F} = t^{-3(n+1)}[-4n(2n-1)$$
$$\times t^{4n}\sqrt{kt^{2-2n}+1}\,{}_2F_1(1/2, 1/(n-1); \quad (18)$$
$$n/(n-1); -kt^{2-2n}) - k^2\left(n^2-1\right)t^4$$
$$+ 2k(n-1)(2n-1)t^{2n+2} + 4n(2n-1)t^{4n}]$$
$$\times [k^3(n-1)(n+1)(3n-1)\sqrt{k+t^{2n-2}}]^{-1}, \quad (19)$$

with $k = v_{\rm orb}^2/(n\sigma)^2$ and ${}_2F_1(a, b; c; z)$ is the hypergeometric function. The integration constant is computed with the condition $\Delta M(t) = 0$ for $t \leq t_0^{\rm acc}$, where $t_0^{\rm acc}$ is the time at which the accretion process starts, namely, the time at which the SN ejecta reaches the NS capture region (see Fig. 26).

3.3. The Reaching of the Critical Mass of the Accreting Companion NS

We discuss now the problem of the maximum stable mass of a NS. Nonrotating NS equilibrium configurations have been recently constructed, by M. Rotondo, J. Rueda, myself and many students, taking into proper account the strong, weak, electromagnetic, and gravitational interactions within general relativity. The equilibrium equations are given by the general relativistic Thomas–Fermi equations coupled with the Einstein–Maxwell equations to form the Einstein–Maxwell–Thomas–Fermi system of equations, which must be solved under the condition of global charge neutrality [140]. These equations supersede the traditional Tolman–Oppenheimer–Volkoff ones that impose the condition of local charge neutrality throughout the configuration. The maximum stable mass $M_{\rm crit} = 2.67M_\odot$ of nonrotating NSs has been obtained in [140]. The high and rapid accretion rate of the SN material can lead the NS mass to reach the critical value $M_{\rm crit} = 2.67M_\odot$. This system will undergo gravitational collapse to a BH, producing a GRB. The initial NS mass is likely to be rather high due to the highly nonconservative mass transfer during the previous history of the evolution of the binary system (see e.g. [128–130], for details). Thus the NS could reach the critical mass in just a few seconds. Indeed we can see from Eq. (15) that for an ejecta density 10^6 g cm^{-3} and velocity 10^9 cm s^{-1}, the accretion rate might be as large as $\dot{M} \sim 0.1\ M_\odot$ s^{-1}. The occurrence of a GRB-SN event in the scenario depends on some specific conditions satisfied by the binary progenitor system, such as a short binary separation and an orbital period <1 h. This is indeed the case with GRB 090618 and 110709B that we have already analyzed within the context of this scenario in [40, 126], respectively (see below in the next subsections). In addition to offering an explanation for the GRB-SN temporal coincidence, the considerations presented here lead

to an astrophysical implementation of the concept of proto-BH, generically introduced in our previous works on GRBs 090618, 970828, and 101023 (see [40, 100, 141]). The proto-BH represents the first stage $20 \lesssim t \lesssim 200$ s of the SN evolution. It is appropriate now to discuss the possible progenitors of such binary systems. A viable progenitor is represented by X-ray binaries such as Cen X-3 and Her X-1 [6, 9, 142–146]. The binary system is expected to follow an evolutionary track [128–130]: the initial binary system is composed of main-sequence stars 1 and 2 with a mass ratio $M_2/M_1 \gtrsim 0.4$. The initial mass of the star 1 is likely $M_1 \gtrsim 11\ M_\odot$, leaving a NS through a core-collapse event. The star 2, now with $M_2 \gtrsim 11\ M_\odot$ after some almost conservative mass transfer, evolves filling its Roche lobe. It then starts a spiralling in of the NS into the envelope of the star 2. If the binary system does not merge, it will be composed of a helium star and a NS in close orbit. The helium star expands filling its Roche lobe and a nonconservative mass transfer to the NS takes place. This scenario naturally leads to a binary system composed of a C + O star and a massive NS, as the one considered here, see Fig. 26. It is clear that after the occurrence of the SN and the GRB emission, the outcome is represented, respectively, by a NS and a BH. If the NS and the BH are gravitationally bound they give rise to a new kind of binary system, which can lead itself to the merging of the NS and the BH and consequently to a new process of gravitational collapse of the NS into the BH. In this case the system could originate yet another process of GRB emission and possibly a predominant emission in gravitational waves.

4. THE APPLICATION OF THE IGC SCENARIO TO GRB 090618

4.1. The SN Ejecta Accretion onto the Companion NS

We recall that the black-body-emitting surface in the first episode evolves during the first ∼32 s, as observed in the rest frame, following a power-law behavior

$$r_{\rm em} = \sigma t^n,$$
$$v_{\rm em} = n\frac{r_{\rm em}}{t} = n\sigma t^{n-1}, \qquad (20)$$

where $\sigma = 8.048 \times 10^8$ cm s^{-n}, $n \approx 3/5$ as shown in Fig. 20, and $v_{\rm em} = dr_{\rm em}/dt \sim 4 \times 10^8$ cm s^{-1} at the beginning of the expansion.

When the mass accreted onto the NS triggers the gravitational collapse of the NS into a BH, the authentic GRB emission is observed in the subsequent episode at $t - t_0 \gtrsim 50$ s (observer frame). The characteristics of GRB 090618 are shown in Table 3 of [39] and we refer to that reference for more details on the GRB light curve and spectrum simulation. We now turn to the details of the accretion process of the SN material onto the NS. We have initially assumed, as an order of magnitude estimate [40], $r_{\rm SN} = r_{\rm em}$ and $v_{\rm SN} = v_{\rm em}$. The NS of initial mass $M_{\rm NS}$ accretes mass from the SN ejecta at a rate given by [99]

$$\dot{M}_{\rm acc}(t) = \pi\rho_{ej}(t)\frac{(2GM_{\rm NS})^2}{v^3_{\rm rel,ej}},$$
$$\rho_{ej}(t) = \frac{3M_{\rm ej}(t)}{4\pi r^3_{\rm SN}(t)}, \qquad (21)$$

where $r^3_{\rm SN}(t)$ given by Eq. (19) and $M_{\rm ej}(t) = M_{\rm ej,0} - M_{\rm acc}(t)$ is the available mass to be accreted by the NS as a function of time, with $M_{\rm ej,0}$ the mass ejected in the SN. $v_{\rm rel,ej} = \sqrt{v^2_{\rm orb} + v^2_{\rm SN}}$ is the velocity of the ejecta relative to the NS, where $v_{\rm SN}$ is the SN ejecta velocity given by Eq. (19) and $v_{\rm orb} = \sqrt{G(M_{\rm core} + M_{\rm NS})/a}$ is the orbital velocity of the NS. Here $M_{\rm core}$ is the mass of the SN core progenitor and a the binary separation. Hereafter we assume $a = 9 \times 10^9$ cm, a value higher than the maximum distance traveled by the SN material during the total time interval of Episode 1, $\Delta t \simeq 32$ s, $\Delta r \sim 7 \times 10^9$ cm (see Fig. 20). If the accreted mass onto the NS is much smaller than the initial mass of the ejecta, i.e., $M_{\rm acc}/M_{\rm ej,0} \ll 1$, the total accreted mass can be obtained from the formula given by Eq. (8) of [99], which for GRB 090618 leads to

$$M_{\rm acc}(t) = \int_{t_0^{\rm acc}}^{t} \dot{M}_{\rm acc}(t)dt$$
$$\approx (2GM_{\rm NS})^2 \frac{15M_{\rm ej,0}t^{2/5}}{8n^3\sigma^6\sqrt{1+kt^{4/5}}}\Bigg|_{t_0^{\rm acc}}^{t}, \qquad (22)$$

where $k = v^2_{\rm orb}/(n\sigma)^2$ and $t_0^{\rm acc}$ is the time at which the accretion process starts, namely, the time at which the SN ejecta reaches the NS capture region, $R_{\rm cap} = 2GM_{\rm NS}/v^2_{\rm rel,ej}$, so for $t \le t_0^{\rm acc}$ we have $M_{\rm acc}(t) = 0$. The accretion process leads to the gravitational collapse of the NS onto a BH when it reaches the critical mass value. Here we adopt the critical mass $M_{\rm crit} = 2.67M_\odot$ computed recently in [140]. Equation (21) is more accurate for massive NSs since the amount of mass needed to reach the critical mass by accretion is much smaller than $M_{\rm ej,0}$. In general, the total accreted mass must be computed from the numerical integration of Eq. (20), which we present below for GRB 090618.

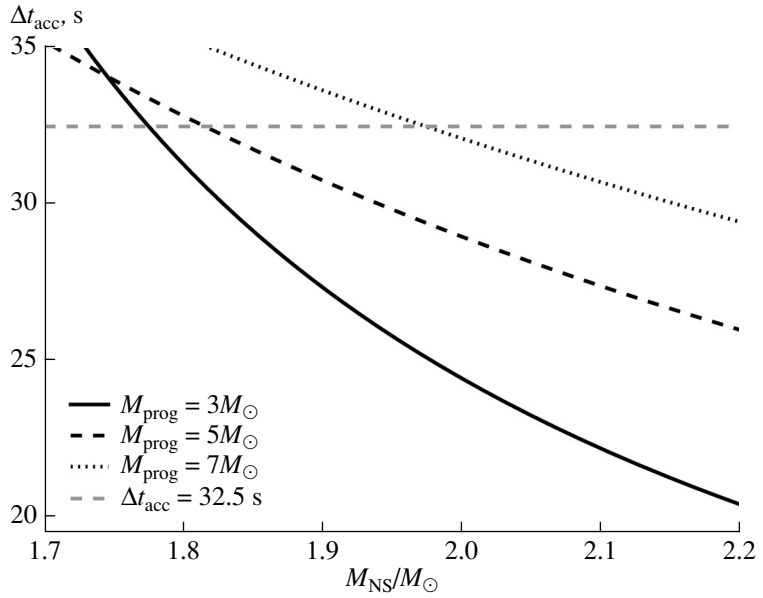

Fig. 27. Time interval Δt_{acc} of the accretion process onto the NS as a function of initial NS mass M_{NS} for selected values of the SN core progenitor mass M_{core}. The horizontal dashed line is the duration $\Delta t = 32.5$ s of the first episode of GRB 090618, which constrains the duration of the time needed by the NS to reach the critical mass. The crossing points between the dashed horizontal line and the solid curves give the NSs with M_{NS} that reach the critical mass in the time Δt. From [40].

4.2. Inferences on the Binary Period

The occurrence of a GRB-SN event in the accretion induced collapse scenario is subject to some specific conditions of the binary progenitor system such as a short binary separation and orbital period. The orbital period in the present case is

$$P = \sqrt{\frac{4\pi^2 a^3}{G(M_{core} + M_{NS})}} = 9.1 \left(\frac{M_{core} + M_{NS}}{M_\odot}\right)^{-1/2} \text{min}. \quad (23)$$

We denote by Δt_{acc} the total time interval since the beginning of the SN ejecta expansion all the way up to the instant where the NS reaches the critical mass. In Fig. 27 we plot Δt_{acc} as a function of the initial NS mass and for different masses of the SN core progenitor mass. The mass of the SN ejecta is assumed to be $M_{ej,0} = M_{core} - M_{rem}$, where M_{rem} is the mass of the central compact remnant (NS) left by the SN explosion. Here we assumed $M_{core} = (3{-}8)M_\odot$ at the epoch of the SN explosion, and $M_{rem} = 1.3M_\odot$, following some of the type Ic SN progenitors studied in [128–130].

We can see from Fig. 27 that, for GRB 090618, the mass of the NS companion that collapses onto a BH should be in the range $1.8 \lesssim M_{NS}/M_\odot \lesssim 2.1$ corresponding to the SN Ic progenitors $3 \leq M_{core}/M_\odot \leq 8$. The massive NS companion of the evolved star is in line with the binary scenario proposed in [134]. These results also agree with the well-understood Ib/c nature of the SN associated with GRBs. The most likely explanation for SN Ib/c, which lack H and He in their spectra, is that the SN progenitor star is in a binary system with an NS; see also [128–130] and also [147, 148]. It is also interesting to compare the results on the IGC of an NS to a BH by a type Ib/c SN [99] with the results of Chevalier [139] on the accretion of a supernova material by the central NS generated by the supernova. A total accreted mass of up to $0.1M_\odot$ in a time of a few hours was obtained there for a normal type II SN. Thus a similar amount of mass can be accreted in the two cases, but in the latter the accretion occurs over a longer time. To reach a high accretion rate of the inner SN material onto the central NS, a mechanism is needed that helps to increase the density of the NS surrounding layers, which is decreasing due to the expansion after being unbound by the SN explosion. Reference [139] analyzed the possibility of having a reverse shock wave as this mechanism while it moves back through the SN core. The reverse shock is formed in the interaction of the mantle gas with the low-density envelope. The time scale of the accretion process is thus determined by the time it takes the reverse shock to reach the vicinity of the central newly born NS, which is a few hours in the case of SN

Fig. 28. Group picture. Standing: Carlo Luciano Bianco, Marco Muccino, Wang Yu. Sitting: Remo Ruffini, Giovani Pisani, Jorge Rueda, Milos Kovacevic, Luca Izzo.

II progenitors. However, the existence of a low-density outer envelope, e.g. H and He outer layers, is essential for the strength of the reverse shock. Fall-back accretion onto the central NS is expected to be relevant only in SN II but not in SN Ic like those associated to GRBs, where H and He are absent.

4.3. The Collapse Time and the Role of Neutrinos

The argument presented in [99] naturally explains the sequence of events: SN explosion—IGC-BH formation—GRB emission. Correspondingly, the accretion of the material ejected by the SN into the nearby NS of the IGC model presented here occurs almost instantaneously. Indeed for the SN expansion parameters obtained from the observations of Episode 1 in GRB 090618 (see Eq. (19)), the accretion of the SN material onto the nearby NS occurs in a few seconds (see Fig. 27). The binary parameters are such that the ejecta density does not decrease too much (from 10^6 to $\sim 10^4$ g cm^{-3}) before reaching the capture region of the NS, leading to a high accretion rate. As pointed out in [139], radiative diffusion will lower the accretion rate up to the Eddington limit (and then to even lower rates) when the trapping radius of the radiation in the flow $r_{\rm tr} = \kappa \dot{M}_{\rm acc}/(4\pi c)$ [139], where κ is the opacity, is equal to the Bondi radius $r_B = GM_{\rm NS}/v^2_{\rm rel,ej}$, the gravitational capture radius. The radius $r_{\rm tr}$ is located where the outward diffusion luminosity is equal to the inward convective luminosity. It can be checked that for the parameters of our system given by Eqs. (19)–(21), the equality $r_{\rm tr} = r_B$ occurs in a characteristic time $\sim$200 days, where we used $\kappa = 0.2$ cm^2 g^{-1}. Thus, this regime is not reached in the present case since the NS is brought to its critical mass just in a few seconds. In the case analyzed by [139], it happens in a time $\sim$8 days. Only recently we have returned to the previously mentioned papers of Zel'dovich and collaborators [24] and Ruffini and Wilson [37], since it is clear that the role of Neutrino emission is essential in the understanding of the accretion process of the SN ejecta into the companion Neutron Star Binary.

It is also a pleasure to insert a picture, see Fig. 28 of the closest collaborators working at ICRANet headquarter in Pescara and at ICRA at the University of Rome "la Sapienza."

5. RECENT HIGHLIGHTS AND THE "THIRD PARADIGM"

Some most recent results have appeared in and are summarized in a "third paradigm," see Figs. 29 and 30:

Third paradigm

- *Long GRBs occur in a "**Cosmic Matrix**" composed by up to 4 different **Episodes**, each one characterized by specific astrophysical processes and Lorentz* Γ *factors (from* $\Gamma \sim 1$ *up to* $\Gamma \sim 10^3$*).*
- *Both Short and Long GRBs with* $E_{iso} > 10^{52}$ *erg originate from a gravitational collapse to a BH (*$M > M_{crit} \sim 2.6 M_\odot$*) and can have GeV emission:*
  - Long GRBs $\longrightarrow$ BdHNe $\longrightarrow$ BH+NS binaries.
  - Short GRBs $\longrightarrow$ Massive BNS mergers $\longrightarrow$ BH.
- *Both Short and Long GRBs with* $E_{iso} < 10^{52}$ *erg do not form BH and have no GeV emission.*
  - Long GRBs $\longrightarrow$ X-Ray Flashes $\longrightarrow$ Hypernovae.
  - Short GRBs $\longrightarrow$ undercritical BNS mergers $\longrightarrow$ Massive NS.

6. ZEL'DOVICH'S REACTION TO THE WORK OF FERMI AND GAMOW

I just mentioned in the introduction that I have considered my finding of the Zel'dovich paper a present from Zel'dovich to our group. I would like to close this article by offering a present to Zel'dovich in this last section. But before I would like to copy from the Book I am preparing "Einstein, Heisenberg and Fermi and the birth of relativistic astrophysics" an anecdote on Zel'dovich and Gamow and also about the side interest of Gamow on Biology. In that book I dedicated a chapter to the Fermi–Turkevich paper and to Gamow work on the hot Big Bang. "One of the most interesting reactions to this entire scientific adventure was that of the Soviet colleagues. I had occasion many times to discuss these issues in unforgettable and most pleasant meetings with Zel'dovich and the outstanding friends around Evgeny Lifshitz in my many visits to Moscow in the 1970s. Let me first recall some of the ongoing work at the time in the Soviet Union. The "rocambolesque" departure of Gamow from Moscow on the occasion of the 1927 Solvay Meeting had embittered all the Soviet scientists who had seen at once all their possibilities to travel abroad cut for years to come. The departure of Gamow was like a slap in the face to the Soviet system (from Chapter 6 of [151]). Motivated by ideological reasons, Zel'dovich told me that in order to prove the superiority of a truly Soviet thinker, he had proposed an alternative way to have a Friedmann universe initially at zero temperature as opposed to Gamow's idea of an initially radiation-dominated hot universe. The avoidance of the buildup of the heavy elements was obtained in the Zel'dovich approach by the existence of a background of degenerate neutrinos. As Zel'dovich says there, "The process $e^- + p = n + \nu$, which leads to the formation of neutrons at high matter density in the stars, turns out to be forbidden here, since the neutrino states that are energetically obtainable in this process are occupied. In the uniform model (closed or open) the neutrinos do not depart anywhere. Upon expansion such a substance turns into pure cold hydrogen" [152]. In this way the formation of neutrons would be completely avoided. The model would lead to a universe formed during its initial evolution uniquely of cold hydrogen. The confrontation was quite clear: a cold universe developed by a Soviet scientist in Soviet Union as opposed to a warm universe developed by a fugitive Soviet scientist abroad! The Zel'dovich approach was soon abandoned, as Igor Novikov told me years later, due to the evidence of the cosmological helium abundance and, more importantly, to the discovery of the cosmological black body radiation (see the Nobel lectures of Arno Penzias and Robert W. Wilson[3] and George T. Smoot[4]). Interestingly, in our discussions (see Fig. 31) following the universal scientific success of the discovery of the cosmological black body radiation, Zel'dovich talked about the role of Gamow in science and politics finishing with one question and one statement. First the question: "How many Nobel Prizes Gamow received? One for physics and one for biology?" Zel'dovich was clearly well informed of the

[3] http://nobelprize.org/nobel_prizes/physics/laureates/1978
[4] http://nobelprize.org/nobel_prizes/physics/laureates/2006

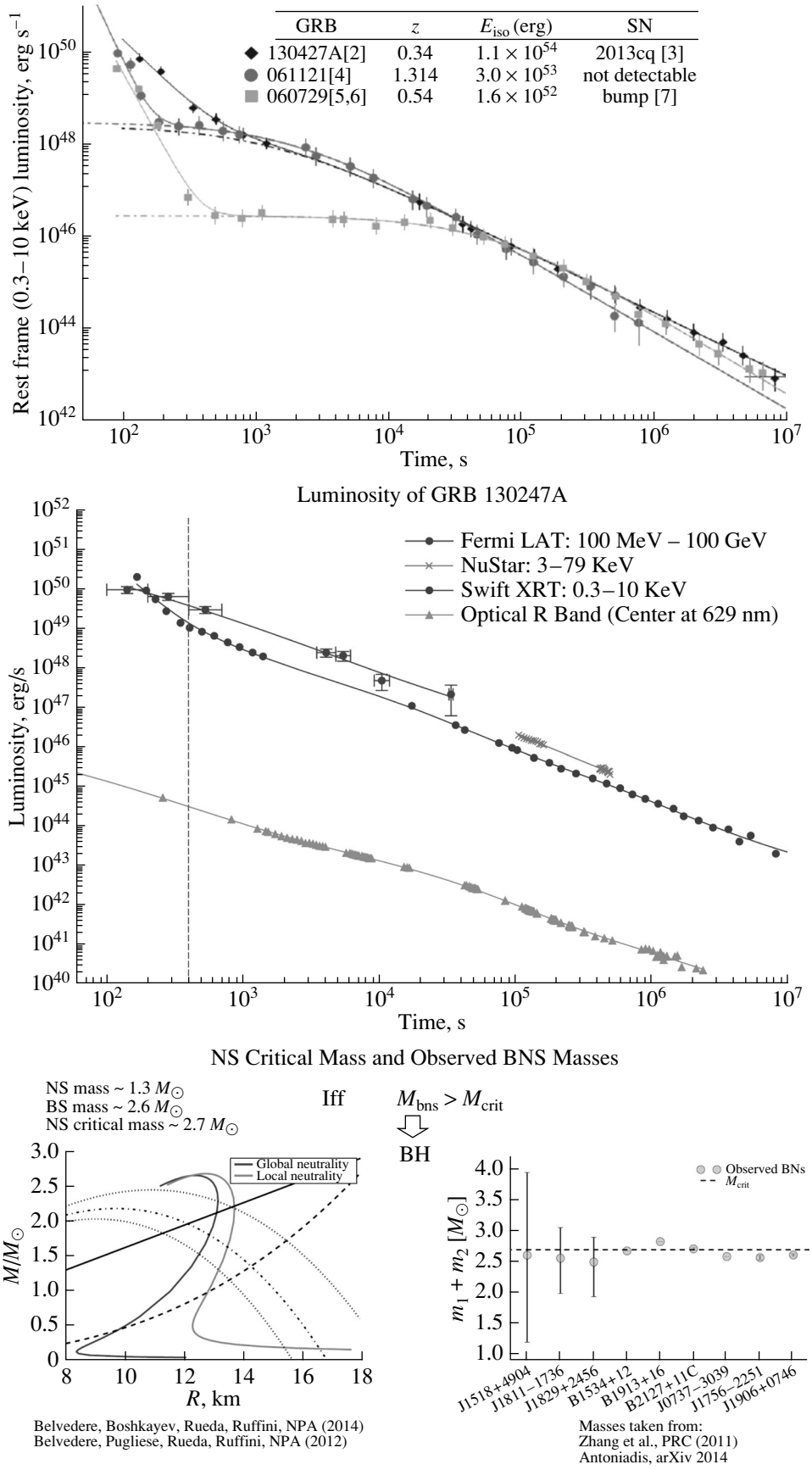

Fig. 29. Top: Episode 3 nesting [97]. Middle: Episode 3 of GRB 130427A, see [98]. Bottom: NS critical mass and observed BNS masses.

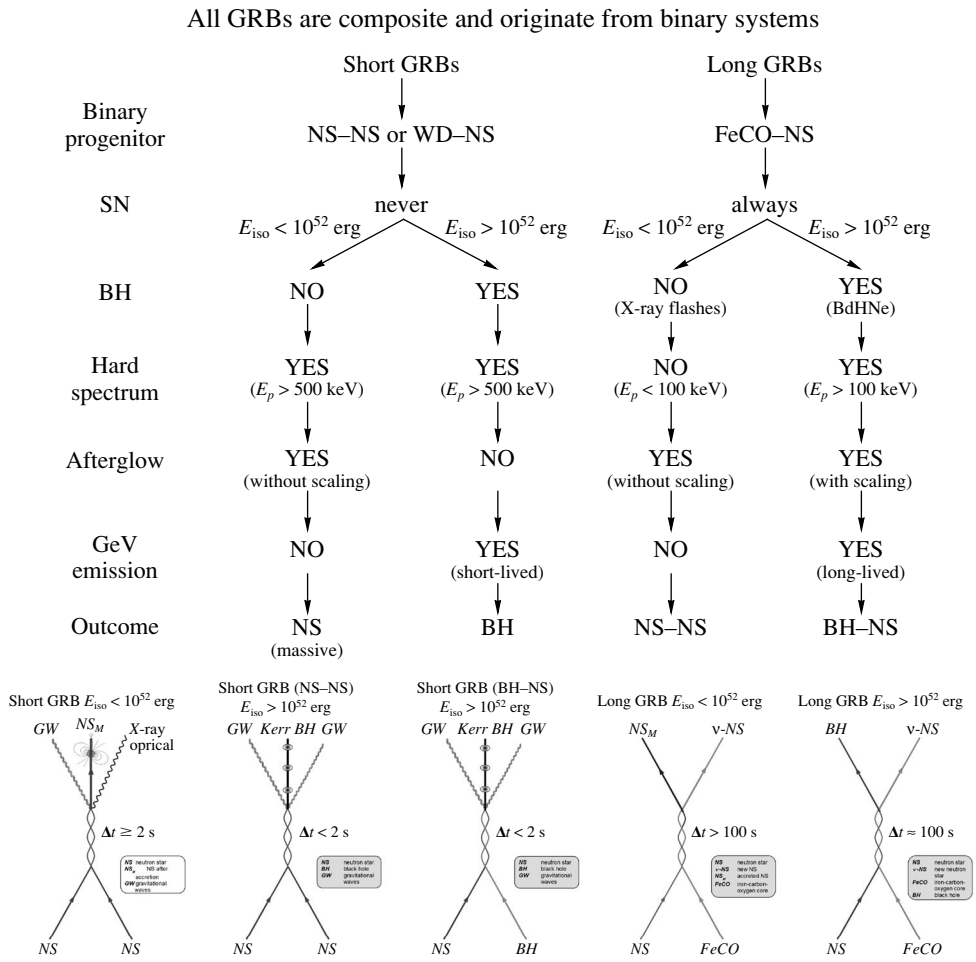

Fig. 30. Top: All GRBs are composite and originate from binary systems, see [98, 149]. Bottom: the five independent "Cosmic Matrix" relating SN and GRBs to their constituent NS and BH.

Fig. 31. Dinner at home of Evgeny Lifshitz. From left to right: Nina Ginzburg (wife of Ginzburg), Zinaida Lifshitz (wife of Lifshitz), Remo Ruffini, Evgeny Lifshitz, Yakov Zel'dovich, Angela Zel'dovich (one of the many wives of Zel'dovich), and Vitalyi Ginzburg.

great contribution of Gamow not only to astrophysics and nuclear physics, but also to biology for his studies on DNA structure [153]. In this question, however, Zel'dovich showed a clear sign of his isolation from the West: Gamow had not received any Nobel prize! Nevertheless he was not ready to give up on the supremacy of Soviet science in view of the universal recognition by then of Gamow's ideas. Smiling he concluded with the statement: "Certainly Gamow has been one of the greatest Soviet scientists." More of my discussion with Zel'dovich is given in [25].

I can then conclude with this essay we recently produced with Pisin Chen: "Did Gamma Ray Burst Induce Cambrian Explosion?" One longstanding mystery in bio-evolution since Darwin's time is the origin of the Cambrian explosion that happened around 540 million years ago (Mya), where an extremely rapid increase of species occurred. Here we suggest that a nearby GRB event 500 parsecs away, which should occur about once per 5 Gy, might have triggered the Cambrian explosion. Due to a relatively lower cross section and the conservation of photon number in Compton scattering, a substantial fraction of the GRB photons can reach the sea level and would induce DNA mutations in organisms protected by a shallow layer of water or soil, thus expediting the biodiversification. This possibility of inducing genetic mutations is unique among all candidate sources for major incidents in the history of bio-evolution. A possible evidence would be the anomalous abundance of certain nuclear isotopes with long half-lives transmuted by the GRB photons in geological records from the Cambrian period. Our notion also imposes constraints on the evolution of exoplanet organisms and the migration of panspermia. Details in [154].

7. CONCLUSIONS

I close with the mention of my paper with Pisin which open a new problematic so fascinating to physics, astrophysics and biology and the meaning and presence of life in our Universe. This a tribute to my two great friends Zel'dovich who I met so many times with always lively discussions at times very close to diversity but always with great admiration and one with Gamow which I never met but always admired as one of the greatest contributors to physics, astrophysics and cosmology. My unconditioned admiration for Gamow was remarked caustically by Wigner who told me "Dr. Ruffini, you admire so much Gamow: Gamow used a special set of units $G = c = h = \pi = 1$!". As I have recently recalled it took me almost forty years to understand this sentence (see the Book I am preparing "Einstein, Heisenberg and Fermi and the Birth of Relativistic Astrophysics" and also [155]), gaining still more respect for Gamow and enjoying the opportunity to probe the unsurpassed elegance of expressing himself of a giant physicist: Eugene Wigner.

ACKNOWLEDGEMENTS

Special acknowledgement for discussions to Lorenzo Amati, Saghar Batebi, Riccardo Belvedere, Carlo Luciano Bianco, Donato Bini, Kuantay Boshkaev, Sheyse Martins de Carvalho, Demetrios Christodoulou, Thibault Damour, Massimo Della Valle, Maxime Enderli, Andrea Geralico, Filippo Frontera, Luca Izzo, Milos Kovacevic, Marco Muccino, Rodrigo Negreiros, Fernanda Gomes De Oliveira, Ana Virginia Penacchioni, Giovani Pisani, Daniela Pugliese, Michael Rotondo, Jorge Rueda, Ivan Siutsou, Seddigheh Tizchang, Aldo Treves, Gregory Vereshchagin, Yu Wang, She-Sheng Xue, Elena Zaninoni.

REFERENCES

1. W. Baade and F. Zwicky, Proc. Natl. Acad. Sci. USA **20**, 254 (1934).
2. W. Baade and F. Zwicky, Proc. Natl. Acad. Sci. USA **20**, 259 (1934).
3. R. Giacconi, H. Gursky, F. R. Paolini, and B. B. Rossi, Phys. Rev. Lett. **9**, 439 (1962).
4. I. S. Shklovsky, Astrophys. J. Lett. **148**, L1 (1967).
5. *Physics and Astrophysics of Neutron Stars and Black Holes, Proceedings of the 75th E. Fermi Summer School,* Ed. by R. Giacconi and R. Ruffini (North-Holland, Amsterdam, 1978).
6. R. W. Leach and R. Ruffini, Astrophys. J. **180**, L15 (1973).
7. C. E. Rhoades and R. Ruffini, Phys. Rev. Lett. **32**, 324 (1974).
8. R. Ruffini, in *Astrophysics and Gravitation, Proceedings of the 16th Solvay Conference on Physics, University of Brussels, September 24–28, 1973* (Univ. Brussels, Brussels, 1973).
9. *Neutron Stars, Black Holes and Binary X-Ray Sources, Proceedings of the Annual Meeting, San Francisco, CA, February 28, 1974,* Ed. by H. Gursky and R. Ruffini, Vol. 48 of *Astrophysics and Space Science Library* (D. Reidel, Dordrecht, 1975).
10. E. Costa, F. Frontera, J. Heise, M. Feroci, J. in't Zand, F. Fiore, M. N. Cinti, D. Dal Fiume, L. Nicastro, M. Orlandini, et al., Nature **387**, 783 (1997).
11. T. Damour and R. Ruffini, Phys. Rev. Lett. **35**, 463 (1975).
12. R. Ruffini, in *Proceedings of the 12th Marcel Grossmann Meeting on General Relativity,* Ed. by T. Damour, R. Jantzen, and R. Ruffini (World Scientific, Singapore, 2012), p. 286.
13. R. Ruffini, in *Proceedings of the 13th Marcel Grossmann Meeting* (2015, in press).

14. R. Ruffini, A. G. Aksenov, M. G. Bernardini, C. L. Bianco, L. Caito, P. Chardonnet, M. G. Dainotti, G. de Barros, R. Guida, L. Izzo, et al., in *Proceedings of the 13th Brazilian School on Cosmology and Gravitation,* Ed. by M. Novello and S. Perez Bergliaffa, AIP Conf. Ser. **1132**, 199 (2009).
15. A. Heger, C. L. Fryer, S. E. Woosley, N. Langer, and D. H. Hartmann, Astrophys. J. **591**, 288 (2003); astro-ph/0212469.
16. E. Verner, F. Bruhweiler, and T. Gull, Astrophys. J. **624**, 973 (2005); astro-ph/0502106.
17. A. Damineli, A. Kaufer, B. Wolf, O. Stahl, D. F. Lopes, and F. X. de Araújo, Astrophys. J. Lett. **528**, L101 (2000); astro-ph/9912387.
18. R. C. Iping, G. Sonneborn, T. R. Gull, D. L. Massa, and D. J. Hillier, Astrophys. J. Lett. **633**, L37 (2005); astro-ph/0510581.
19. E. Pian, L. Amati, L. A. Antonelli, R. C. Butler, E. Costa, G. Cusumano, J. Danziger, M. Feroci, F. Fiore, F. Frontera, et al., Astrophys. J. **536**, 778 (2000).
20. S. R. Kulkarni, D. A. Frail, M. H. Wieringa, R. D. Ekers, E. M. Sadler, R. M. Wark, J. L. Higdon, E. S. Phinney, and J. S. Bloom, Nature (London) **395**, 663 (1998).
21. T. J. Galama, P. M. Vreeswijk, J. van Paradijs, C. Kouveliotou, T. Augusteijn, H. Böhnhardt, J. P. Brewer, V. Doublier, J.-F. Gonzalez, B. Leibundgut, et al., Nature **395**, 670 (1998).
22. R. Ruffini, G. Vereshchagin, and S. Xue, Phys. Rep. **487**, 1 (2010); arXiv:0910.0974.
23. R. Ruffini, Y. Wang, M. Kovacevic, C. L. Bianco, M. Enderli, M. Muccino, A. V. Penacchioni, G. B. Pisani, and J. A. Rueda; arXiv:1405.5723 (2014).
24. Y. B. Zeldovich, L. N. Ivanova, and D. K. Nadyozhin, Sov. Astron. **16**, 209 (1972).
25. R. Ruffini, in *The Sun, the Stars, the Universe and General Relativity,* Ed. by R. Ruffini and G. V. Vereshchagin, AIP Conf. Ser. **1205**, 1 (2010); arXiv:0911.4825.
26. A. Hewish, S. J. Bell, J. D. H. Pilkington, P. F. Scott, and R. A. Collins, Nature **217**, 709 (1968).
27. W. Arnett, in *From Nuclei to White Dwarfs and Neutron Stars,* Ed. by A. Mezzacappa and R. Ruffini (World Scientific, Singapore, in press).
28. M. Rees, R. Ruffini, and J. A. Wheeler, *Black Holes, Gravitational Waves and Cosmology: An Introduction to Current Research,* Vol. 10 of *Topics in Astrophysics and Space Physics* (Gordon and Breach, Science Publ., New York, 1974).
29. A. Finzi and R. A. Wolf, Astrophys. J. **153**, 865 (1968).
30. D. Christodoulou and R. Ruffini, Phys. Rev. D **4**, 3552 (1971).
31. R. Ruffini, in *The Kerr Spacetime*, Ed. by D. L. Wiltshire, M. Visser, and S. Scott (Cambridge Univ. Press, 2009).
32. R. Ruffini, J. D. Salmonson, J. R. Wilson, and S.-S. Xue, Astron. Astrophys. **350**, 334 (1999).
33. R. Ruffini, J. D. Salmonson, J. R. Wilson, and S.-S. Xue, Astron. Astrophys. **359**, 855 (2000).
34. R. Ruffini, in *Fluctuating Paths and Fields,* Ed. by W. Janke, A. Pelster, H. J. Schmidt, and M. Bachmann (World Scientific, Singapore, 2001).
35. W. S. Paciesas, C. A. Meegan, G. N. Pendleton, M. S. Briggs, C. Kouveliotou, T. M. Koshut, J. P. Lestrade, M. L. M Collough, J. J. Brainerd, J. Hakkila, et al., Astrophys. J. Suppl. Ser. **122**, 465 (1999).
36. F. Frontera, in *Proceedings of the 13th Marcel Grossmann Meeting* (2015, in press).
37. R. Ruffini and J. Wilson, Phys. Rev. Lett. **31**, 1362 (1973).
38. *Physics and Astrophysics of Neutron Stars and Black Holes,* Ed. by R. Giacconi and R. Ruffini (Cambridge Scientific Publishers, 2009).
39. L. Izzo, R. Ruffini, A. V. Penacchioni, C. L. Bianco, L. Caito, S. K. Chakrabarti, J. A. Rueda, A. Nandi, and B. Patricelli, Astron. Astrophys. **543**, A10 (2012); arXiv:1202.4374.
40. L. Izzo, J. A. Rueda, and R. Ruffini, Astron. Astrophys. **548**, L5 (2012), 1206.2887.
41. G. B. Pisani, L. Izzo, R. Ruffini, C. L. Bianco, M. Muccino, A. V. Penachioni, J. A. Rueda, and Y. Wang, Astron. Astrophys. **552**, L5 (2013); arXiv:1304.1764.
42. M. Muccino, R. Ruffini, C. L. Bianco, L. Izzo, and A. V. Penachioni, Astrophys. J. **763**, 125 (2013); arXiv:1205.6600.
43. T. Piran, Rev. Mod. Phys. **76**, 1143 (2004); arXiv:astro-ph/0405503.
44. G. Cavallo and M. J. Rees, Mon. Not. R. Astron. Soc. **183**, 359 (1978).
45. J. Goodman, Astrophys. J. **308**, L47 (1986).
46. B. Paczynski, Astrophys. J. **308**, L43 (1986).
47. P. Meszaros, Rep. Prog. Phys. **69**, 2259 (2006).
48. R. Ruffini, G. Vereshachagin, and S. Xue, Phys. Rep. **487**, 1 (2010); arXiv:0910.0974.
49. R. Ruffini, Int. J. Mod. Phys. D **20**, 1797 (2011); arXiv:1107.0862.
50. R. Ruffini, in *Black Holes and High Energy Astrophysics,* Ed. by H. Sato and N. Sugiyama, Vol. 23 of *Frontiers Science Series* (Universal Academic Press, Tokyo, 1998), p. 167.
51. G. Preparata, R. Ruffini, and S.-S. Xue, Astron. Astrophys. **338**, L87 (1998).
52. A. Aksenov, R. Ruffini, and G. Vereshchagin, Phys. Rev. Lett. **99**, 125003 (2007).
53. E. Ramirez-Ruiz and E. E. Fenimore, Astrophys. J. **539**, 712 (2000); arXiv:astro-ph/9910273.
54. M. J. Rees and P. Meszaros, Astrophys. J. **430**, L93 (1994).
55. M. J. Rees and P. Meszaros, Mon. Not. R. Astron. Soc. **258**, 41P (1992).
56. M. Tavani, Astrophys. J. **466**, 768 (1996).
57. F. Frontera, L. Amati, E. Costa, J. M. Muller, E. Pian, L. Piro, P. Soffitta, M. Tavani, A. Castro-Tirado, D. Dal Fiume, et al., Astrophys. J. Suppl. Ser. **127**, 59 (2000).

58. A. Crider, E. P. Liang, I. A. Smith, R. D. Preecce, M. S. Briggs, G. N. Pendleton, W. S. Paciesas, D. L. Band, and J. L. Matteson, Astrophys. J. **479**, L39 (1997).
59. R. D. Preecce, M. S. Briggs, T. W. Giblin, R. S. Mallozzi, G. N. Pendleton, W. S. Paciesas, and D. L. Band, Astrophys. J. **581**, 1248 (2002).
60. G. Ghirlanda, A. Celotti, and G. Ghisellini, Astron. Astrophys. **393**, 409 (2002).
61. G. Ghirlanda, A. Celotti, and G. Ghisellini, Astron. Astrophys. **406**, 879 (2003); arXiv:astro-ph/0210693.
62. P. Kumar and E. M Mahon, Mon. Not. R. Astron. Soc. **384**, 33 (2008), 0802.2704.
63. T. Piran, R. Sari, and Y. Zou, Mon. Not. R. Astron. Soc. **393**, 1107 (2009).
64. R. D. Blandford and C. F. M Kee, Phys. Fluids **19**, 1130 (1976).
65. E. Molinari, S. D. Vergani, D. Malesani, S. Covino, P. D'Avanzo, G. Chincarini, F. M. Zerbi, L. A. Antonelli, P. Conconi, V. Testa, et al., Astron. Astrophys. **469**, L13 (2007); arXiv:astro-ph/0612607.
66. E. S. Rykoff, F. Aharonian, C. W. Akerlof, M. C. B. Ashley, S. D. Barthelmy, H. A. Flewelling, N. Gehrels, E. Göğüş, T. Güver, Ü. Kiziloğlu, et al., Astrophys. J. **702**, 489 (2009).
67. R. Sari and T. Piran, Astrophys. J. **520**, 641 (1999); arXiv:astro-ph/9901338.
68. G. Ghisellini and A. Celotti, Astron. Astrophys. Suppl. **138**, 527 (1999); arXiv:astro-ph/9906145.
69. A. A. Zdziarski, R. Svensson, and B. Paczynski, Astrophys. J. **366**, 343 (1991).
70. A. Shemi, Mon. Not. R. Astron. Soc. **269**, 1112 (1994); arXiv:astro-ph/9404047.
71. A. Pe'er and B. Zhang, Astrophys. J. **653**, 454 (2006); arXiv:astro-ph/0605641.
72. M. V. Medvedev, Astrophys. J. **540**, 704 (2000); arXiv:astro-ph/0001314.
73. A. Panaitescu and P. Mészáros, Astrophys. J. **544**, L17 (2000); arXiv:astro-ph/0009309.
74. B. E. Stern and J. Poutanen, Mon. Not. R. Astron. Soc. **352**, L35 (2004); arXiv:astro-ph/0405488.
75. D. Eichler and A. Levinson, Astrophys. J. **529**, 146 (2000); arXiv:astro-ph/9903103.
76. P. Mészáros and M. J. Rees, Astrophys. J. **530**, 292 (2000); arXiv:astro-ph/9908126.
77. P. Mészáros, Ann. Rev. Astron. Astrophys. **40**, 137 (2002).
78. F. Daigne and R. Mochkovitch, Mon. Not. R. Astron. Soc. **336**, 1271 (2002); arXiv:astro-ph/0207456.
79. D. Giannios, Astron. Astrophys. **457**, 763 (2006); arXiv:astro-ph/0602397.
80. F. Ryde and A. Pe'er, Astrophys. J. **702**, 1211 (2009); arXiv:0811.4135.
81. D. Lazzati and M. C. Begelman, Astrophys. J. **725**, 1137 (2010); arXiv:1005.4704.
82. R. Ruffini, Astron. Astrophys. Suppl. **138**, 513 (1999).
83. R. Ruffini, C. L. Bianco, P. Chardonnet, F. Fraschetti, and S.-S. Xue, Astrophys. J. **555**, L113 (2001).
84. C. L. Bianco and R. Ruffini, Astrophys. J. **605**, L1 (2004).
85. C. L. Bianco and R. Ruffini, Astrophys. J. **620**, L23 (2005).
86. P. Meszaros, P. Laguna, and M. J. Rees, Astrophys. J. **415**, 181 (1993).
87. R. Sari, Astrophys. J. **489**, L37 (1997).
88. R. Sari, Astrophys. J. **494**, L49 (1998).
89. E. Waxman, Astrophys. J. **491**, L19 (1997).
90. M. J. Rees and P. Meszaros, Astrophys. J. **496**, L1 (1998).
91. J. Granot, T. Piran, and R. Sari, Astrophys. J. **513**, 679 (1999).
92. A. Panaitescu and P. Meszaros, Astrophys. J. **493**, L31 (1998).
93. A. Gruzinov and E. Waxman, Astrophys. J. **511**, 852 (1999).
94. J. van Paradijs, C. Kouveliotou, and R. A. M. J. Wijers, Ann. Rev. Astron. Astrophys. **38**, 379 (2000).
95. C. L. Bianco and R. Ruffini, Astrophys. J. **633**, L13 (2005).
96. R. Ruffini, C. L. Bianco, P. Chardonnet, F. Fraschetti, and S.-S. Xue, Astrophys. J. **555**, L117 (2001).
97. R. Ruffini, M. Muccino, C. L. Bianco, M. Enderli, L. Izzo, M. Kovacevic, A. V. Penachioni, G. B. Pisani, J. A. Rueda, and Y. Wang, Astron. Astrophys. **565**, L10 (2014); arXiv:1404.3946.
98. R. Ruffini, Y. Wang, M. Enderli, M. Muccino, M. Kovacevi , C. L. Bianco, A. V. Penachioni, G. B. Pisani, and J. A. Rueda, Astrophys. J. **798**, 10 (2015), 1405.5723.
99. J. A. Rueda and R. Ruffini, Astrophys. J. **758**, L7 (2012).
100. A. V. Penacchioni, R. Ruffini, L. Izzo, M. Muccino, C. L. Bianco, L. Caito, B. Patricelli, and L. Amati, Astron. Astrophys. **538**, A58 (2012); arXiv:1112.2970.
101. R. Ruffini, L. Izzo, A. V. Penacchioni, C. L. Bianco, L. Caito, S. K. Chakrabarti, and A. Nandi, PoS. (Texas2010), 101 (2011).
102. P. Schady, W. H. Baumgartner, A. P. Beardmore, S. Campana, P. A. Curran, C. Guidorzi, J. A. Kennea, J. Mao, R. Margutti, J. P. Osborne, et al., GCN Circ. **9512** (2009).
103. W. H. Baumgartner, S. D. Barthelmy, J. R. Cummings, E. E. Fenimore, N. Gehrels, H. A. Krimm, C. B. Markwardt, D. M. Palmer, T. Sakamoto, G. Sato, et al., GCN Circ. **9530**, 1 (2009).
104. G. J. Fishman, C. A. Meegan, R. B. Wilson, M. N. Brock, J. M. Horack, C. Kouveliotou, S. Howard, W. S. Paciesas, M. S. Briggs, G. N. Pendleton, et al., Astrophys. J. Suppl. Ser. **92**, 229 (1994).
105. A. P. Beardmore and P. Schady, GCN Circ. **9528**, 1 (2009).

106. C. Meegan, G. Lichti, P. N. Bhat, E. Bissaldi, M. S. Briggs, V. Connaughton, R. Diehl, G. Fishman, J. Greiner, A. S. Hoover, et al., Astrophys. J. **702**, 791 (2009).
107. D. Band, J. Matteson, L. Ford, B. Schaefer, D. Palmer, B. Teegarden, T. Cline, M. Briggs, W. Paciesas, G. Pendleton, et al., Astrophys. J. **413**, 281 (1993).
108. S. M Breen, GCN Circ. **9535** (2009).
109. S. B. Cenko, D. A. Perley, V. Junkkarinen, M. Burbidge, U. S. Diego, and K. Miller, GCN Circ. **9518** (2009).
110. B. E. Schaefer, Astrophys. J. **660**, 16 (2007); arXiv:astro-ph/0612285.
111. S. Golenetskii, R. Aptekar, E. Mazets, V. Pal'shin, D. Frederiks, P. Oleynik, M. Ulanov, D. Svinkin, and T. Cline, GCN Circ. **9553**, 1 (2009).
112. K. Kono, A. Daikyuji, E. Sonoda, N. Ohmori, H. Hayashi, K. Noda, Y. Nishioka, M. Yamauchi, M. Ohno, M. Suzuki, et al., GCN Circ. **9568**, 1 (2009).
113. F. Longo, E. Moretti, G. Barbiellini, E. Vallazza, M. Trifoglio, A. Bulgarelli, F. Gianotti, F. Fuschino, M. Marisaldi, C. Labanti, et al., GCN Circ. **9524** (2009).
114. Y. Kotov, A. Kochemasov, S. Kuzin, V. Kuznetsov, J. Sylwester, and V. Yurov, in *Proceedings of the 37th COSPAR Scientific Assembly, Montreal, July 2008* (2008), p. 1596.
115. A. Nandi, A. R. Rao, S. K. Chakrabarti, J. P. Malkar, S. Sreekumar, D. Debnath, M. K. Hingar, T. Kotoch, Y. Kotovk, and A. Arkhangelskiy; arXiv:0912.4126 (2009).
116. A. R. Rao, J. P. Malkar, M. K. Hingar, V. K. Agrawal, S. K. Chakrabarti, A. Nandi, D. Debnath, T. B. Kotoch, R. Sarkar, T. R. Chidambaram, et al., Astrophys. J. **728**, 42 (2011); arXiv:1012.0641.
117. Z. Cano, D. Bersier, C. Guidorzi, R. Margutti, K. M. Svensson, S. Kobayashi, A. Melandri, K. Wiersema, A. Pozanenko, A. J. van der Horst, et al., Mon. Not. R. Astron. Soc. **413**, 669 (2011); arXiv:1012.1466.
118. F. Ryde, M. Axelsson, B. B. Zhang, S. M. Glynn, A. Pe'er, C. Lundman, S. Larsson, M. Battelino, B. Zhang, E. Bissaldi, et al., Astrophys. J. **709**, L172 (2010); arXiv:0911.2025.
119. S. Guiriec, V. Connaughton, M. S. Briggs, M. Burgess, F. Ryde, F. Daigne, P. Mészáros, A. Goldstein, J. M. Enery, N. Omodei, et al., Astrophys. J. **727**, L33 (2011); arXiv:1010.4601.
120. A. Pe'er, Astrophys. J. **682**, 463 (2008); arXiv:0802.0725.
121. C. Cherubini, A. Geralico, H. J. A. Rueda, and R. Ruffini, Phys. Rev. D **79**, 124002 (2009).
122. R. Ruffini, C. L. Bianco, P. Chardonnet, F. Fraschetti, L. Vitagliano, and S.-S. Xue, in *Cosmology and Gravitation,* Ed. by M. Novello and S. E. Perez Bergliaffa (2003), AIP Conf. Ser. **668**, 16 (2003).
123. C. L. Fryer, J. A. Rueda, and R. Ruffini, Astrophys. J. **793**, L36 (2014); arXiv:1409.1473.
124. R. Ruffini, M. G. Bernardini, C. L. Bianco, L. Caito, P. Chardonnet, M. G. Dainotti, F. Fraschetti, R. Guida, G. Vereshchagin, and S.-S. Xue, in *Proceedings of the 6th Integral Workshop on the Obscured Universe,* Ed. by S. Grebenev, R. Sunyaev, C. Winkler, A. Parmar, and L. Ouwehand, vol. SP-622 of *ESA Special Publication* (2007), p. 561.
125. B. Patricelli, M. G. Bernardini, C. L. Bianco, L. Caito, L. Izzo, R. Ruffini, and G. Vereshchagin, Int. J. Mod. Phys. D **20**, 1983 (2011).
126. A. V. Penacchioni, R. Ruffini, C. L. Bianco, L. Izzo, M. Muccino, G. B. Pisani, and J. A. Rueda, Astron. Astrophys. **551**, A133 (2013); arXiv:1301.6014.
127. J. Hjorth and J. S. Bloom, in *Gamma-Ray Bursts,* Cambridge Astrophysics Series, Vol. 51, Ed. by C. Kouveliotou, R. A. M. J. Wijers, and S. E. Woosley (Cambridge Univ. Press, 2012), pp. 169–190.
128. K. Nomoto and M. Hashimoto, Phys. Rep. **163**, 13 (1988).
129. K. Nomoto, H. Yamaoka, O. R. Pols, E. P. J. van den Heuvel, K. Iwamoto, S. Kumagai, and T. Shigeyama, Nature **371**, 227 (1994).
130. K. Iwamoto, K. Nomoto, P. Höflich, H. Yamaoka, S. Kumagai, and T. Shigeyama, Astrophys. J. **437**, L115 (1994).
131. S. E. Woosley and J. S. Bloom, Ann. Rev. Astron. Astrophys. **44**, 507 (2006).
132. A. Shemi and T. Piran, Astrophys. J. **365**, L55 (1990).
133. T. Piran, A. Shemi, and R. Narayan, Mon. Not. R. Astron. Soc. **263**, 861 (1993).
134. R. Ruffini, M. G. Bernardini, C. L. Bianco, L. Caito, P. Chardonnet, C. Cherubini, M. G. Dainotti, F. Fraschetti, A. Geralico, R. Guida, et al., in *Proceedings of the 11th Marcel Grossmann Meeting,* Ed. by H. Kleinert, R. T. Jantzen, and R. Ruffini (World Scientific, Singapore, 2008), p. 368; arXiv:0804.2837.
135. R. Ruffni, M. G. Bernardini, C. L. Bianco, L. Vitagliano, S.-S. Xue, P. Chardonnet, F. Fraschetti, and V. Gurzadyan, in *Proceedings of the 10th Marcel Grossmann Meeting,* Ed. by M. Novello, S. Perez Bergliaffa, and R. Ruffini (World Scientific, Singapore, 2006), p. 369.
136. O. D. Toropina, M. M. Romanova, and R. V. E. Lovelace, Mon. Not. R. Astron. Soc. **420**, 810 (2012); arXiv:1111.2460.
137. H. Bondi and F. Hoyle, Mon. Not. R. Astron. Soc. **104**, 273 (1944).
138. F. Hoyle and R. A. Lyttleton, Proc. Cambridge Philos. Soc. **35**, 405 (1939).
139. R. A. Chevalier, Astrophys. J. **346**, 847 (1989).
140. R. Belvedere, D. Pugliese, J. A. Rueda, R. Ruffini, and S.-S. Xue, Nucl. Phys. A **883**, 1 (2012); arXiv:1202.6500.
141. L. Izzo, R. Ruffini, C. L. Bianco, H. Dereli, M. Muccino, A. V. Penacchioni, G. Pisani, and J. A. Rueda; arXiv:1205.6651 (2012).

142. E. Schreier, R. Levinson, H. Gursky, E. Kellogg, H. Tananbaum, and R. Giacconi, Astrophys. J. **172**, L79 (1972).
143. R. E. Wilson, Astrophys. J. **174**, L27 (1972).
144. H. Tananbaum, H. Gursky, E. M. Kellogg, R. Levinson, E. Schreier, and R. Giacconi, Astrophys. J. **174**, L143 (1972).
145. K. Davidson and J. P. Ostriker, Astrophys. J. **179**, 585 (1973).
146. M. L. Rawls, J. A. Orosz, J. E. McClintock, M. A. P. Torres, C. D. Bailyn, and M. M. Buxton, Astrophys. J. **730**, 25 (2011); arXiv:1101.2465.
147. A. V. Tutukov and A. V. Fedorova, Astron. Rep. **51**, 291 (2007).
148. R. A. Chevalier, Astrophys. J. **752**, L2 (2012); arXiv:1204.3300.
149. M. Muccino, R. Ruffini, M. Kovacevic, L. Izzo, F. G. Oliveira, J. A. Rueda, C. L. Bianco, M. Enderli, A. V. Penacchioni, G. B. Pisani, et al.; arXiv:1412.1018 (2014).
150. R. Ruffini, L. Izzo, M. Mucino, G. B. Pisani, J. A. Rueda, Y. Wang, C. Barbarino, C. L. Bianco, M. Enderli, and M. Kovacevic, Astron. Astrophys. **569**, A39 (2014); arXiv:1404.1840.
151. G. Gamow, *My World Line: An Informal Autobiography* (Viking Press, New York, NY, 1970).
152. Y. B. Zeldovich, Sov. Phys. JETP **16**, 1102 (1963).
153. G. Gamow, Nature **173**, 318 (1954).
154. P. Chen and R. Ruffini; arXiv:1403.7303 (2014).
155. H. Ludwig and R. Ruffini, J. Korean Phys. Soc. **65**, 892 (2014); arXiv:1402.3691.